Boosting The Peripheral Immune Response in the Skeletal Muscles Improved Motor Function in ALS Transgenic Mice

Maria Chiara Trolese
Mario Negri Institute for Pharmacological Research Branch of Milan: Istituto di Ricerche Farmacologiche Mario Negri

Carlotta Scarpa
Mario Negri Institute for Pharmacological Research Branch of Milan: Istituto di Ricerche Farmacologiche Mario Negri

Valentina Melfi
Mario Negri Institute for Pharmacological Research Branch of Milan: Istituto di Ricerche Farmacologiche Mario Negri

Paola Fabbrizio
Mario Negri Institute for Pharmacological Research Branch of Milan: Istituto di Ricerche Farmacologiche Mario Negri

Francesca Sironi
Mario Negri Institute for Pharmacological Research Branch of Milan: Istituto di Ricerche Farmacologiche Mario Negri

Martina Rossi
Mario Negri Institute for Pharmacological Research Branch of Milan: Istituto di Ricerche Farmacologiche Mario Negri

Caterina Bendotti
Mario Negri Institute for Pharmacological Research Branch of Milan: Istituto di Ricerche Farmacologiche Mario Negri

Giovanni Nardo (giovanni.nardo@marionegri.it)
Istituto Di Ricerche Farmacologiche Mario Negri https://orcid.org/0000-0002-1803-1484

Research article

Keywords: amyotrophic lateral sclerosis, mouse models, skeletal muscle, satellite cells, macrophages, myogenesis, motor neuron

Posted Date: October 13th, 2021

DOI: https://doi.org/10.21203/rs.3.rs-929588/v1

Abstract

Background: Monocyte chemoattractant protein 1 (MCP1/CCL2) is one of the most powerful pro-inflammatory chemokines. However, its signalling is pivotal in driving axonal and muscle regeneration following injury.

We previously showed that MCP1 is strongly upregulated in the nervous system of slow-progressing than fast-progressing SOD1^{G93A} mice, which are characterised by a poor immune response that leads to a massive nerve and muscle degeneration.

Methods: To assess the MCP1-mediated therapeutic role, we boosted the chemokine along the motor unit of the two SOD1^{G93A} ALS models through a single intramuscular injection of a scAAV9 vector engineered with the *Mcp1* gene (scAAV9_MCP1) at the pre-symptomatic disease stage.

Results: Our observations revealed that slow-progressing SOD1^{G93A} mice responded positively to the scAAV9_MCP1 injection anticipating the activation of the immune response, which sustained the pro-regenerative programme within nerves and skeletal muscles, eventually slackening the symptoms progression. Conversely, fast-progressing SOD1^{G93A} mice exhibited an adverse response to the treatment, exacerbating the toxic inflammatory response in the periphery, resulting in worsened motor ability late in the disease.

Intriguingly, our data suggested a novel pleiotropic role of MCP1 in the nervous system of SOD1^{G93A} mice capable of promoting axon regeneration and modulating neuroinflammation, with the overall effect of preventing neurodegeneration.

Conclusions: We provided direct evidence underlying the pivotal role of the immune response in promoting and governing skeletal muscle regeneration and thus the speed of ALS progression. The comparison study performed in fast- and slow-progressing SOD1^{G93A} mice spotlights the nature and temporal activation of the inflammatory response as limiting factors to protect the peripheral compartment and interfere with the disease course tangibly. Altogether, these observations highlight the immune response as a key determinant for disease variability and proffer a reasonable explanation for the failure of systemic immunomodulatory treatments suggesting new potential strategies to hamper ALS progression.

Background

Amyotrophic lateral sclerosis (ALS) is a fatal motor neuron (MN) disease characterised by degenerative changes in upper and lower motor neurons. All over the world, it is one of the most common neuromuscular disorders across all ethnicities, with an incidence of 2-3 cases per 100.000 individuals per year [1]. Onset typically occurs in late middle life and presents as relentlessly progressive muscle atrophy and weakness, with the effects on respiratory muscles limiting survival to 2–4 years after disease onset in most cases [1]. The diagnosis is based on clinical assessment of symptoms, with a delay of more than

a year from symptom onset, quite beyond the therapeutic window of disease-modifying drugs [1]. Around 10% of patients have a familial form of the disease, and mutations in 20 different genes have been associated with ALS development. The genes most frequently implicated are *sod1*, *fus*, *tardbp* and *c9orf72*. The remaining 90% of cases are sporadic with an unknown aetiology [2].

The main obstacle to gain full insight into the pathogenesis of ALS is the remarkable clinical heterogeneity of the disease phenotype and course, even in patients carrying the same mutation [3,4], and the multisystemic nature of ALS pathology, which distinctively encompasses remote biological systems and makes the identification of a proper therapeutic target even more challenging [5,6].

Over the last 20 years, the use of mutant SOD1 (mSOD1) mice has allowed identifying several mechanisms that contribute to MN injury [7]. However, this remarkable body of knowledge did not yield the expected outcomes in terms of therapeutic benefits. Indeed, both pharmacological and genetic interference with apoptotic pathways in the MN cell body only marginally affects mSOD1 mice lifespan [8,9], suggesting that MN protection alone is insufficient to prevent peripheral axons and muscles from degenerating.

The denervation atrophy of skeletal muscles is an early event in the ALS pathogenic cascade, anticipating symptoms manifestation [10,11]. Studies in transgenic mSOD1 mice showed that muscle atrophy occurs before any clear signs of MN degeneration. This evidence has led to ALS being reviewed as a distal axonopathy whereby skeletal muscles actively contribute to a retrograde signalling cascade that culminates with the MN death [12]. Moreover, it has emerged that certain aspects of ALS are non-cell-autonomous and that other cell types within the spinal cord, including microglia, astrocytes, and T-cells, contribute to the progression of the disease [13,14].

Mounting evidence highlighted the distinct contribution of the inflammatory response in the central nervous system (CNS) with respect to the periphery (i.e. nerves and muscles) in ALS [15,16]. Indeed, while the aberrant glial cells activation, T cells infiltration and the resulting release of pro-inflammatory molecules drive neurodegeneration, successful axon and muscle regeneration depends on the coordinated efforts of immune cells that, besides removing cellular debris, release factors that support the wound healing [17–20]. This may explain the association between the peripheral nervous system (PNS) inflammation and the longer disease duration recently observed in ALS patients with SOD1 mutation [21].

This evidence indicates that the immune response can actively influence the disease progression, promoting phenomena of protection and/or toxicity [22,23]. Therefore, shed light on the temporal and mechanistic involvement of the immune response in the different compartments affected by the disease will be a practical approach to discover new biomarkers and identify targets for developing precise therapeutic strategies to ameliorate ALS progression.

We recently characterised two mouse strains (C57 and 129Sv) carrying the same copies of human mutant SOD1 transgene ($SOD1^{G93A}$) but exhibiting remarkable differences in terms of disease

progression and overall survival [24,25]. We found that, despite the same extent of MN loss during the disease progression [24], the fast-progressing mice (129SvSOD1^{G93A}) showed earlier muscle denervation and higher axonal dysregulation that correlated with a poor inflammatory response and reduced macrophages infiltration in the periphery [26,27] compared with the slow-progressing ALS mice (C57SOD1^{G93A}). Further analyses showed that fast-progressing ALS mice failed to activate Monocyte Chemoattractant Protein 1 (MCP1) in MN perikarya and peripheral axons compared to C57SOD1^{G93A} mice [26,28]. This evidence suggests that MCP1 signalling and immune cell recruitment might be pivotal in delaying muscular denervation and triggering regeneration in the PNS [29,30], thus regulating the speed of the disease progression of the two ALS models.

MCP1 is an 8 kDa secretory protein, usually released to exert a potent pro-inflammatory effect by binding the specific CCR2 on its target cells. MCP1/CCR2-mediated signalling drives the downstream phosphatidylinositol-3 kinase / Akt and MAPK pathways, and it is known that this axis induces chemotaxis of monocytes/macrophages [31,32], microglia [33], lymphocytes [34–36] and neutrophils [37], leading to pathological microgliosis and inflammatory activation in chronic disorders [38].

MCP1 levels are increased in serum and cerebrospinal fluid of sporadic and familial ALS patients [39]. Besides, studies in mSOD1 mice have shown that MCP1 is significantly upregulated in the spinal cord and peripheral nerves at the early disease stage, suggesting a pathogenic role of this chemokine [26,40]. Nonetheless, several evidence depicted MCP1 as a neuroprotective factor involved in modulating the blood-brain-barrier permeability [41], promoting the differentiation of neural progenitors [42,43] and axonal elongation [44,45]. Moreover, the chemotactic activity of MCP1 towards macrophages and T cells is crucial in wound healing and regenerative processes of nerves [46–48] and muscles [29,49–53] following acute trauma.

While the effective role of immune cell recruitment in the PNS is still controversial [15,16,54,55], no experimental inference is available on the immune response in skeletal muscles during ALS course.

In the present study, we investigated the therapeutic efficacy of a scAAV9 vector engineered with the *Mcp1* gene injected in the skeletal muscles of fast and slow progressing SOD1^{G93A} mice. We found that an early boosting of immune response in the peripheral compartment is crucial in countering the denervation atrophy and slowing down the ALS progression in slow- but not fast-progressing mSOD1 mice. Moreover, our data described a pleiotropic role of MCP1 in the CNS as a protective factor, able to modulate the neuroinflammation, possibly reducing the MN loss. This evidence is instrumental in comprehending the contribution of the immune response in ALS, shedding light on its worth in governing the speed of the disease progression.

Methods

Mice

Female transgenic SOD1^{G93A} mice on C57BL/6J (stock no: 004435; The Jackson Laboratories) or 129SvHsd genetic background, hereafter indicated as C57SOD1^{G93A} and 129SvSOD1^{G93A}, respectively, and corresponding non-transgenic (Ntg) littermates were used. Transgenic SOD1^{G93A} mice expressing ~20 copies of mutant human SOD1 with a Gly93Ala substitution (B6SJL-TgSOD1^{G93A}-1Gur) were initially obtained from Jackson Laboratories and maintained on a C57BL/6JOlaHsd (C57) genetic background at Harlan Italy S.R.L., Bresso, Milan, Italy. From the crossbreeding of C57BL/6JOlaHsd (C57SOD1^{G93A}) with 129S2/SvHsd (129Sv) for >15 generations, we obtained SOD1^{G93A} mice on the homogenous background 129SSv (129SvSOD1^{G93A}).

All animal procedures have been performed according to the following laws, regulations, and policies governing the care and use of laboratory animals: Italian Governing Law (D.lgs 26/2014; Authorisation n.19/2008-A issued March 6, 2008 by Ministry of Health); Mario Negri Institutional Regulations and Policies providing internal authorisation for persons conducting animal experiments (Quality Management System Certificate – UNI EN ISO 9001:2015 – Reg. N° 6121); the NIH Guide for the Care and Use of Laboratory Animals (2011 edition) and EU directives and guidelines (EEC Council Directive 2010/63/UE). Mice were housed 4/5 per standard cages in specific pathogen-free and controlled environmental conditions (temperature: 22±2°C; relative humidity: 55±10% and 12 h of light). Food (standard pellets) and water were supplied ad libitum.

Intra-muscular administration of scAAV9 vector

Engineered (gfp or mcp1) or "empty" self-complementary Adeno-associated virus serotype 9 (scAAV9) vectors were purchased by Virovek (Hayward, CA, USA). To ensure a high expression of the transgene (gfp or mcp1), the constitutive cytomegalovirus (CMV) promoter was used.

Adult (6 or 8 weeks-old) SOD1^{G93A} mice underwent a single bilateral intramuscular injection of 2,18x1010 vg/µL of the scAAV9 vector. The scAAV9 opportunely diluted in sterile PBS was injected in both hindlimb (Tibialis Anterior, TA; Gastrocnemius Caput Medialis, GCM; Gluteus Maximus, GM) and forelimb (Triceps Brachii, TB) muscles following the protocol previously described by Gruntman et al. [56]*. Briefly, mice were anaesthetised with isoflurane inhalation, fur shaved to visualise the target muscles, and a 30-gauge needle was inserted in the muscle centre to inject the scAAV9 (10µL/muscle). Mice were divided into the treated (scAAV9_MCP1) and control (scAAV9_(empty)) groups through a block-randomisation in which the blocks are defined on the body weight, sex and sibling separation.*

Behavioural analysis

Starting from 8 weeks of age, motor onset and disease progression were monitored bi-weekly in C57SOD1^{G93A} and 129SvSOD1^{G93A} scAAV9-treated mice by a blind operator recording the body weight and the motor performance at the paw grip endurance (PaGE) test. In the PaGE test, mice are placed on a horizontal grid at 30 cm height, and the tail is gently pulled until they grasp the grid with their fore and hind paws. The grid is gently turned upside down, and the latency time of the mouse to fall on the table is

recorded for a maximum of 90s. Each mouse is given up to three attempts, and the most prolonged latency is recorded. The onset of muscle strength deficit is considered when the mice showed the first signs of impairment in the PaGE test. In C57SOD1^{G93A} mice, the latency was evaluated as previously described [57]*; conversely, in 129SvSOD1^{G93A} animals, the performance obtained in the grip strength test was assessed through a score, calculated as indicated by Lauranzano et al.* [58].

Immunohistochemical analysis

Mice were anaesthetised with a mix of ketamine (1.75 mg/Kg) and medetomidine (1 mg/Kg) and transcardially perfused with 50 ml of 0.1M PBS pH 7.4. Following the blood removal, skeletal muscles (TA, GCM, GM and TB) and nerves were dissected and immediately frozen in cooled isopentane or n-pentane, respectively. At the same time, the vertebral column was post-fixed overnight in a solution of 4% paraformaldehyde in 0.1M PBS. The following day the vertebrae were removed, and the spinal cord was transferred to 30% sucrose solution with 0.1% sodium azide in 0.1 M PBS at 4°C for cryoprotection before mounting in optimal cutting temperature compound (Tissue-Tek, Sakura).

The following primary antibodies and staining were used: chicken anti-GFP (1:750, GTX13970 GeneTex); rat anti-MCP1 (1:50, ab8101 Abcam); rabbit anti-Iba1 (1:500, 019-19741 Fujifilm Wako); mouse anti-GFAP (1:2500, MAB3402 Merck Millipore); goat anti-ChAT (1:200, AB144P Merck Millipore); rat anti-macrosialin (CD68, 1:200, MCA1957 BioRad); Neurotrace conjugated with Alexa-647 (1:500; N21483 Invitrogen); mouse anti-S100β (1:400; AMAB91038 Sigma-Aldrich); mouse anti-phosphorylated neurofilament H (Smi31, 1:5000; 801608 BioLegend); rabbit anti-neurofilament heavy polypeptide (NF200, 1:1000; N4142 Sigma-Aldrich); rat anti-CD11b (1:200; MCA74G BioRad); rabbit anti-iNOS (1:200, PA3-030A Invitrogen); rabbit anti-mannose receptor (CD206, 1:200, ab64693 Abcam); mouse anti-Pax7 (1:400, AB_528428 DSHB); rabbit anti-MyoD (1:100, PA5-23078 Invitrogen); rabbit anti-neutrophils elastase (1:300, ab68672 Abcam); Hoechst (1:1000; Roche). Alexa Fluor™- 488, 594 and 647 secondary antibodies (Invitrogen) were used with a dilution of 1:500. All immunohistochemistry was done following an indirect immunostaining protocol at room temperature except primary antibody staining, which was performed at 4°C over night.

Spinal cord immunohistochemistry was done on free-floating sections (30 µm), then mounted on glass slides (Waldemar Knittle) with Fluorsave (Calbiochem). Cryosections of nerves (14 µm) or skeletal muscles (20 µm, longitudinal; 12 µm, coronal) were treated directly on poly-lysine objective slides (VWR International) and then mounted with Fluorsave (Calbiochem).

Fluorescence-labelled spinal cord sections were analysed under a sequential scanning mode to avoid bleed-through effects with an IX81 microscope equipped with a confocal scan unit FV500 with three laser lines: Ar-Kr (488 nm), He-Ne red (646 nm), and He-Ne green (532 nm) (Olympus, Tokyo, Japan) and a UV diode using a 10x objective. For lumbar motor neurons count (one every ten sections), a total of 12 serial ChAT-stained sections were analysed. The neuron areas were analysed with Fiji software (Image J, U. S. NIH, Bethesda, Maryland, USA). As previously indicated [59]*, only neuronal somas with an area ≥ 400µm^2 were considered for quantitative analysis of MN numbers. Fluorescence-labelled sections images (3/5 per*

animal) of the Tibialis Anterior and Triceps Brachii muscle were analysed with an Olympus virtual slide system VS110 (Olympus, Center Valley, USA) and acquired at 20x magnification. A systematic random sampling procedure was applied as previously described [57,60]. *Briefly, a grid of equivalent sampling fields was outlined on the muscle slice profile. To ensure that every part of the slice had an equal chance of being sampled, a bidimensional stereological sampling procedure was applied analysing equivalent fields placed at a fixed distance from each other on the tissue slice, using the "grid" function in Fiji (Image J, U. S. NIH, Bethesda, Maryland, USA). The same approach was used to evaluate the neutrophil elastase staining by calculating the percentage of covered area (Area fraction %) per field for each section in the analysis with Fiji software.*

Morphometric analysis of muscles

Tibialis Anterior and Triceps Brachii muscles were dissected out and snap-frozen in liquid nitrogen. For the muscle fibres composition (SDH staining), 10 µm-thickness serial coronal cryosections from the mid-belly region of the TA muscle were air-dried and then incubated at 37°C for 30' in phosphate buffer (0.2 M, pH 7.6) containing 13.5 mg/mL Na-succinate (Sigma-Aldrich) and 0.5 mg/mL of nitro blue tetrazolium (Sigma-Aldrich, 0.29 mg/mL of buffer solution). After staining, sections were fixed with 4% paraformaldehyde, dehydrated in 15% alcohol for 5' and finally mounted with DPX compound (Sigma-Aldrich).

For the muscle fibre cross-sectional area, 10 µm-thickness serial coronal cryosections from the mid-belly region of the TA muscle were air-dried, fixed in 4% paraformaldehyde solution for 5', and stained with Wheat Germ Agglutinin, Alexa Fluor™ 488 Conjugate (1:500; W11261 Thermo Fisher) and Hoechst (1:1000; Roche).

Images were acquired with an Olympus virtual slide system VS110 (Olympus, Center Valley, USA) at 20x magnification and analysed through Fiji (Image J, U.S. NIH, Bethesda, Maryland, USA) on 3/5 serial sections per animal. For the SDH staining, a systematic random sampling procedure was applied as described above. For the muscle fibre cross-sectional area and centralised nuclei, the entire TA or TB muscles section was analysed with the "MuscleJ" plug-in of Fiji software as previously described [61].

Muscle denervation and terminal motor axons sprouting

Tibialis Anterior muscles were dissected out and snap-frozen in liquid nitrogen. Six serial longitudinal cryosections (20 µm-thickness) per animal were analysed. Muscle sections were stained with mouse anti-synaptic vesicle glycoprotein 2A (SV2, 1:50; SV2 DSHB), mouse anti-neurofilament medium polypeptide (2H3, 1:100; AB_2314897 DSHB) and rabbit anti-growth associated protein 43 (GAP43, 1:100; [62]*) following a classic indirect staining protocol. α-bungarotoxin (α-BTX) coupled to Alexa Fluor™ 594 (1:500; B13423 Invitrogen) was incubated for 1h at room temperature. Images were obtained with Nikon A1 confocal scan unit (Nikon Corporation, Japan) at 20X-magnification. The co-localisation channel between neurofilament (SV2/2H3), GAP43 and α-BTX immunostaining was produced for each Z-stack. The percentage of innervated NMJs was quantified considering the overlap between neurofilaments*

(SV2/2H3) staining and a-BTX labelled endplates. The regenerating terminal motor axons rate was calculated based on the co-localisation between neurofilaments (SV2/2H3), GAP43 staining and a-BTX labelled endplates. The analyses were performed by NIS elements software (Nikon Corporation, Japan).

Western blot

Mice were anaesthetised with a mix of ketamine (1.75 mg/Kg) and medetomidine (1 mg/Kg) and transcardially perfused with 50ml of 0.1M PBS pH7.4. Following blood removal, skeletal muscles were dissected out and immediately frozen in cooled isopentane. The spinal cord was fluxed from the vertebral column employing sterile physiological solution (0.9% NaCl) and dissected in the three main segments (i.e. cervical, thoracic and lumbar). Spinal cord segments and nerves were immediately frozen on dry ice. Protein lysates were obtained by homogenisation of mice skeletal muscles, sciatic nerves and spinal cords in lysis buffer as previously described [57]. *Briefly, tissues were powdered in liquid nitrogen then homogenised by sonication in ice-cold homogenisation buffer (Tris HCl pH 8 50 mM, NaCl 150 mM, EGTA pH 8.5 mM, MgCl2 1.5 mM, Triton x-100 1%, anhydrous glycerol 10%, phosphatases and proteases inhibitor cocktail Roche), centrifuged at 13000 rpm for 15 min at 4°C and the supernatants were collected and stored at -80°C.*

Equal amounts of total protein homogenates were loaded on polyacrylamide gels and electroblotted onto PVDF membrane (Millipore) using Trans-Blot Turbo Transfer System (BioRad). After saturation with blocking agent, membranes were immunoblotted with the following primary antibodies: chicken anti-GFP (1:5000, GTX13970 GeneTex); mouse anti-GAPDH (1:10000, CB1001 Merck Millipore); mouse anti-β-actin (1:30000; MAB1501 Merck Millipore); rabbit anti-Arginase1 (1:1000, ab91279 Abcam); mouse anti-gp91^{PHOX} (1:1000, 611415 BD); mouse anti-GFAP (1:30000, MAB3402 Merck Millipore); rabbit anti-Iba1 (1:1000, 019-19741 Fujifilm Wako); goat anti-p75^{NTR} (1:1000, sc-271708 Santa Cruz); rabbit anti-NF200 (1:4000, N4142 Sigma-Aldrich); rat anti-MBP (1:1000, aa82-87 Biorad), mouse anti-SIRT1 (1:750, S5196 Sigma-Aldrich), mouse anti-Pax7 (1:1000, AB_528428 DSHB), rabbit anti-MyoD (1:5000, PA5-23078 Invitrogen); mouse anti-MyoG (1:350, AB_2146602 DSHB) followed by HRP-conjugated secondary antibodies (Thermo Fisher) and developed with Luminata Forte Western Chemiluminescent HRP Substrate (Millipore) at ChemiDoc™ Imaging Systems (BioRad). The optical density of the blots was measured with Image Lab 6.1 software (BioRad) and normalised to the total amount of protein loaded stained with Ponceau S solution (Sigma-Aldrich)[63] *unless otherwise specified.*

Real-Time PCR

Tissues (spinal cords, sciatic nerves and muscles) were freshly collected and immediately frozen on dry ice after mouse perfusion with 0.1 M PBS. The total RNA from tissues was extracted using the Trizol method (Invitrogen) and purified with PureLink RNA columns (Thermo Fisher) following the manufacturer's instructions. RNA samples were treated with DNase I, and reverse transcription was done with a High Capacity cDNA Reverse Transcription Kit (Thermo Fisher).

For Real-time PCR, we used the Taq Man Gene expression assay (Applied Biosystems) following the manufacturer's instructions on cDNA specimens in triplicate, using SensiFAST Probe Hi-ROX Kit (BioLine) and 1x mix containing the specific probes (Thermo Fisher). The following probes (Thermo Fisher) were used for the real-time PCR assay: MCP1 (Mcp1, Mm00441242_m1); cholinergic receptor nicotinic gamma subunit (Chrng, Mm00437419_m1); CD8 alpha receptor (CD8a; Mm01182107_g1); CD4 alpha receptor (CD4a; Mm00442754_m1); Forkhead box P3 (Foxp3; Mm00475162_m1); Insulin-like Growth Factor 1 (Igf1; Mm00439560_m1); Tumour Necrosis Factor-alpha (Tnfα, Mm00443258_m1); Macrosialin (CD68; Mm03047343_m1); Interleukin 4 (Il4, Mm00445259_m1); Interleukin 1 beta (Il1β, Mm00434228_m1). Relative quantification was calculated from the ratio between the cycle number (Ct) at which the signal crossed a threshold set within the logarithmic phase of the given gene and that of the reference β-actin gene (Mm02619580_g1). Mean values of the triplicate results for each animal were used as individual data for the Livak relative gene expression analysis ($2^{-\Delta\Delta Ct}$).

Statistical analysis

All the statistical analyses were performed using Prism 9 for Windows (GraphPad Software Inc.). Values are reported as mean ± SEM. For each analysis, the dependant and group variable are respectively named on the y- and x-axis of the graph.

The sample size for behavioural analysis was defined according to the "Guidelines for preclinical animal research in ALS/MND: A consensus meeting" [64]*. Parameters (body weight and PaGe test) used to evaluate disease progression in $SOD1^{G93A}$ mice were analysed by repeated-measures ANOVA followed by Sidak's post-analysis. Symptoms onset was analysed by Log-rank Mantel-Cox test, and Kaplan-Meier plots were generated.*

Mean values ± standard deviation were used for statistical analysis by Student's t-test for two groups or by One-way ANOVA followed by Fisher's multiple comparison test for more than two groups. In the case of two independent variables, two-way ANOVA followed by Fisher's LSD multiple comparison test was performed. D'Agostino & Pearson omnibus normality test and relative QQ plots were used to assess the assumption of normality. In the event of populations with unequal variance, the Brown-Forsythe ANOVA test followed by the unpaired t-test with Welch's correction was applied.

*For all analyses, a p-value < 0.05 was considered statistically significant. The asterisk * indicates the comparison with the non-transgenic littermates, while the dot ° indicates the comparison between scAAV9_MCP1- and scAAV9_(empty)-treated mice. Further details, including p-values and number of samples, are documented in the Results, Figures, and relative captions.*

Results

MCP1 is more expressed in the central and peripheral nervous system of C57$SOD1^{G93A}$ than 129Sv$SOD1^{G93A}$ mice

We previously found that MCP1 was significantly upregulated by MNs and peripheral axons of slow-progressing than fast-progressing SOD1^{G93A} mice at the disease onset [26,28]. The immunohistochemical analysis supported the higher activation of MCP1 in the spinal cord of C57SOD1^{G93A} compared with 129SvSOD1^{G93A} model (**Fig. 1A, B**), confirming the chemokine expression by MNs (**Fig. 1C**, **D; Supplementary Fig. 1A-C**) and microglia (**Supplementary Fig. 1D-F**) but not astrocytes (**Supplementary Fig. 1G-I**) in the CNS of mSOD1 mice [40]. Notably, a temporal change in the chemokine expression pattern was found in C57SOD1^{G93A} as the disease progresses, characterised by a significant MCP1 expression by microglia and MNs at the pre-symptomatic and onset disease stage, respectively, followed by a widespread activation at the advanced phases (**Fig. 1E**). Specularly, immunohistochemical analysis revealed a progressive increase of MCP1 expression in the sciatic nerve of C57SOD1^{G93A} mice as the disease progresses (**Fig. 1F**) by motor axons and Schwann cells (**Supplementary Fig. 1J, K**).

The specific induction of MCP1 within the motor unit ameliorated the disease progression of C57SOD1^{G93A} mice

To hit the neuromuscular system of ALS mice, we selected the self-complementary adeno-associated virus serotype 9 (scAAV9) in light of its ability to target the spinal cord hijacking the axonal transport machinery and travel along the nerve following intramuscular (i.m.) injection [65]. A single bilateral i.m. injection of the scAAV9 expressing the enhanced *Green Fluorescent Protein* gene (scAAV9_GFP) under the Cytomegalovirus (CMV) promoter efficiently transduced the motor unit in adult C57 and 129Sv mSOD1 mice, as demonstrated by the GFP expression in the skeletal muscles (**Supplementary Fig. 2A-C**), motor axons (**Supplementary Fig. 2D-F**), and spinal cord of scAAV9_GFP treated mice (**Supplementary Fig. 2G-J**). Notably, in the CNS, the transduction occurred specifically within MN perikarya without affecting the neighbouring non-neuronal cells (**Supplementary Fig. 2G', H'**).

To analyse the effect of the MCP1 boosting on the disease progression, the scAAV9 vector properly engineered with the murine sequence of *Mcp1* (scAAV9_MCP1) was injected in the hindlimb (*Gastrocnemius Caput Medialis*, GCM; *Tibialis Anterior*, TA; *Gluteus Maximus*, GM) and forelimb (*Triceps Brachii*, TB) skeletal muscles of pre-symptomatic (8 weeks-old) C57SOD1^{G93A} mice (**Fig. 2A**). Given the early muscle deficit in mSOD1 mice [66,67], eight mice per group were sacrificed ~two weeks before the motor onset (14 weeks), whilst ten mice were monitored until the symptomatic disease stage (20 weeks). A scAAV9(empty) vector was used as control (**Fig. 2A**).

During the study, no difference in the body weight was observed between the two experimental groups, excluding any major side effect upon the induction of a pro-inflammatory factor in ALS mice (**Fig. 2B**). Notably, in the scAAV9_MCP1 treated mice the impairment of muscle strength was delayed and progressed slowly up to 20 weeks of age (**Fig. 2C**), leading to the postponement of the disease onset of ~2 weeks compared with the control group (Empty 16±0.8 weeks, MCP1 18.6±0.4 weeks. mean±SEM) (**Fig. 2D**).

The MCP1 boosting in the hindlimb skeletal muscles of C57SOD1^{G93A} mice delayed the denervation atrophy and prompted muscle re-innervation

The impairment of skeletal muscles is an early event in the ALS pathogenic cascade [68–70], pivotal in determining the motor ability of mSOD1 mice. To dissect the effect of the MCP1 boosting on muscular degeneration, we first investigated the TA muscle given the advanced susceptibility of the lower motor units in mSOD1 mice [71] and the high composition in fast-fatigable fibres, which are early affected by the disease [66,72]. In keeping with the ameliorated clinical phenotype, at 14 weeks, the TA muscle of scAAV9_MCP1-treated mice was less jeopardised (**Fig. 3A**). Our analysis recorded a reduction of 38.8±2.6% (mean±SEM) of the muscle mass in the scAAV9(empty)-treated mice compared with non-transgenic (Ntg) littermates, which decreased at 25.9±2.3% (mean±SEM) upon scAAV9_MCP1 injection. Moreover, a significant downregulation of the foetal gamma-subunit of the acetylcholine receptor (*AChRγ*) was recorded upon MCP1 induction, indicating considerable preservation of muscle innervation compared with the scAAV9(empty)-treated mice [73] (**Fig.3B**). Accordingly, the histological analysis revealed a reduced percentage of denervated neuro-muscular junctions (NMJs) in the hind paw muscle of scAAV9_MCP1- compared with the scAAV9(empty)-treated mice (**Supplementary Fig. 3A, C**). Intriguingly, the histological examination uncovered a higher proportion of motor axons expressing the Growth Associated Protein 43 (GAP43) upon MCP1 boosting, indicating the reinstatement of the nerve sprouting in the fast-twitch muscle of SOD1^{G93A} mice [74,75] (**Supplementary Fig. 3A, D**). A higher rate of GAP43^{+} regenerating motor axons and innervated NMJs was still detectable in the scAAV9_MCP1-treated group at the symptomatic disease stage (**Supplementary Fig. 3B-D**), albeit without impinge on the *AChRγ* transcription level nor TA muscle atrophy compared with the control group (**Fig. 3A, B**). Altogether these data align with previous evidence suggesting maladaptive axonal sprouting in mSOD1 mice as the disease progresses [76,77].

The early MCP1 boosting favoured the establishment of an anti-inflammatory milieu in the skeletal muscles of C57SOD1^{G93A} mice

Multiple evidence correlates the protective effect of the MCP1-mediated inflammation to its chemoattractant activity towards immune cells, particularly macrophages [29,49,78], which are pivotal at sustaining skeletal muscle healing upon damage [79]. Accordingly, we next analysed the chemokine levels within the TA muscle of the scAAV9_MCP1-treated and control group at the pre-symptomatic and symptomatic disease stages. *Mcp1* transcript resulted significantly upregulated in the TA muscle of C57SOD1^{G93A} mice compared with the NTg littermates at 20 but not 14 weeks of age and dramatically increased by scAAV9_MCP1 injection at both time points (**Fig. 3C**). Notably, the extent of chemokine induction recorded in scAAV9_MCP1-treated mice at 14 and 20 weeks of age was similar, confirming the ability of the scAAV9 at inducing the chemokine several weeks after the single i.m. injection (FC *vs* Ntg 14wks: 548.8±81.7; 20wks: 542.1±82.5. mean±SEM). Accordingly, we found a significant increase in the recruitment of phagocytic CD68^{+} macrophages within the TA muscle of scAAV9_MCP1-treated mice

compared with the control groups. This effect was significant at 14 but not 20 weeks of age, when macrophages massively infiltrate the skeletal muscle of mSOD1 mice [80] (**Fig. 3D-F**).

Therefore, we investigated the inflammatory fingerprint acquired by the MCP1-recruited immune cells in the skeletal muscle of 14 weeks-old C57SOD1^{G93A} mice. The histological analysis revealed that the percentage of the M1 iNOS^{+} myeloid cells infiltrated in the TA muscle significantly dropped upon MCP1 boosting, whereas a remarkably increase of the M2 CD206^{+} counterpart was recorded compared with the scAAV9(empty)-treated mice (**Fig. 4 A-D**). The examination of the muscular inflammatory milieu in the scAAV9_MCP1 treated mice revealed a significant downregulation of the Insulin-like Growth Factor 1 (*Igf1*) compared with the control group (**Fig. 4E**), a cytokine released by M1-macrophages exerting an autocrine function pivotal to trigger the M2-gene programme [81]. In keeping with this, in the TA muscle of scAAV9_MCP1-treated mice, we found a higher increase of Sirtuin 1 (Sirt1) deacetylase protein level (**Fig. 4H**), whose overexpression in skeletal muscle is associated with macrophage polarisation shift towards the anti-inflammatory phenotype [82,83]. This, together with the significant *Tumour necrosis factor*-α (T*nf*α) downregulation (**Fig. 4F**) and increased Arginase 1 (Arg1) expression (**Fig. 4G**), indicated the establishment of an anti-inflammatory environment in the hind paw muscle of C57SOD1^{G93A} mice six weeks after the scAAV9_MCP1 injection.

CCR2 is also expressed by activated T lymphocytes [84], instrumental in the regenerative mechanisms of skeletal muscles [52]. The analysis of *CD4* and *CD8a* transcripts did not reveal any difference between the two groups of C57SOD1^{G93A} mice (**Supplementary Fig. 4A, B**), whilst significant upregulation of *FoxP3* transcript was recorded upon MCP1 induction, suggesting an increased infiltration of T regulatory lymphocytes (T regs) compared with the scAAV9(empty) group (**Supplementary Fig. 4C**). As indicated by the fine kinetic governing the immune response within the injured muscle [53,85,86], T regs are the last immune cells infiltrating into the injured tissue pivotal at sustaining the pro-healing programme [87,88]. Altogether, this evidence suggests that the MCP1 induction has anticipated the physiological immune response within the hind paw muscles of C57SOD1^{G93A} mice. In keeping with this, a reduced release of the elastase enzyme was recorded in the TA muscle of scAAV9_MCP1-treated mice compared with the control group (**Supplementary Fig. 4D, E**), indicating that neutrophils, which are the first immune cells recruited by the chemotactic gradient established within the damaged muscle [85,89,90], have already given way to leucocytes.

Despite the significant *Mcp1* upregulation (**Fig. 3C**), no difference in macrophages (**Fig. 3D, F**) and T cells (**Supplementary Fig. 4A-C**) recruitment was found within the TA muscle of scAAV9_MCP1- and scAAV9(empty)-treated mice at 20 weeks of age. Besides, no variation was registered in the inflammatory response between the two experimental groups other than a significant reduction in *Igf1* levels (**Supplementary Fig. 4F**) and the **Cytochrome b-245 heavy chain** (gp91^{PHOX}) expression in the scAAV9_MCP1-treated group (**Supplementary Fig. 4G, H**).

The early MCP1-mediate boosting of the immune response triggered myogenic progenitor cell differentiation in the hindlimb skeletal muscle of C57 SOD1^{G93A} mice

The ability of recruited immune cells at governing the myogenic programme upon damage is strictly dependent on the acquired inflammatory fingerprint. While the M1-macrophages promote activation and proliferation of the myogenic progenitors, their switch towards the M2 phenotype is fundamental to sustain the final commitment of satellite cells (SCs) towards myogenesis [85,91–94].

We showed that scAAV9_MCP1 injection anticipated the immune response in the TA muscle of C57SOD1^{G93A} mice, favouring the establishment of an anti-inflammatory pro-regenerative milieu. Therefore, we next assessed the impact of MCP1 boosting on the expression of two critical myogenic factors in the TA muscle of 14 weeks-old C57SOD1^{G93A} mice: Paired Box 7 (Pax7), the hallmark of SCs stemness [95], and Myogenin (MyoG), a marker of early commitment and differentiation [96]. MyoG, but not Pax7, resulted significantly upregulated in the TA muscle of scAAV9_MCP1-treated mice compared with the control group (**Fig. 5A-C**). Besides, our analysis revealed that the expression of the Myoblast Determination protein 1 (MyoD), a transcription factor critical at defining the activated SCs fate [97,98], was significantly increased upon MCP1 boosting (**Fig. 5A, D**). Suitably, the histological examination showed a reduction in the percentage of quiescent (Pax7^{+}/MyoD^{-}) and a significant increase of differentiating (Pax7^{-}/MyoD^{+}) SCs in the TA muscle of scAAV9_MCP1-treated mice compared with controls (**Supplementary Fig. 5A, D**). According to the increased myogenic activity, a higher percentage of centralised myonuclei was recorded in the hind paw muscle of C57SOD1^{G93A} mice upon MCP1 boosting (% Vs Ntg: 191.0±54.7, Empty; 380.7±44.2, MCP1. mean±SEM), indicating an intense regenerative process compared with the scAAV9(empty) group [99] (**Supplementary Fig. 5B, E**).

Given that the shift from large fast-twitch to small slow-twitch fibres is a common hallmark of ALS [100,101], we next estimated the TA oxidative muscle fibre composition by the succinic dehydrogenase (SDH) histochemical assay. As expected, SOD1^{G93A} mice exhibited a higher percentage of slow-twitch oxidative fibres (87.3±1.4%, mean±SEM) compared with Ntg littermates (52.9±0.1%, mean±SEM), which significantly decreased upon MCP1 boosting (74.7±1.9%, mean±SEM) (**Supplementary Fig. 5C, F**). In keeping with this, the TA muscle fibres mean cross-sectional area (CSA) was higher in the scAAV9_MCP1-treated mice compared with the control group (**Fig. 5E, F**). Besides, the histological analysis revealed a significant reduction in the percentage of the small (<205μm^2) and compensatory preservation of medium (1000-2000μm^2) fibres in the TA muscle of C57SOD1^{G93A} mice upon MCP1 boosting (**Fig. 5E, G**).

Altogether, this evidence suggests a possible correlation between the M2 polarisation of the muscular inflammatory milieu and the enhanced myogenic activity in the TA muscle of the scAAV9_MCP1-treated mice. This effect progressively weakened during the disease progression as, at 20 weeks, we did not record any differences between the two groups of SOD1^{G93A} mice in the myogenic programme, despite the significant *Mcp1* upregulation in the skeletal muscles (**data not shown**).

The MCP1-mediated boosting preserved motor axon from demyelination in the sciatic nerves of C57SOD1^{G93A} mice

We previously reported an association between the activation of the MCP1-mediated pathway in the PNS and a slower disease progression of SOD1^{G93A} mice [26]. Therefore, we analysed the effect of MCP1 induction and the eventual immune cell recruitment within the sciatic nerve of C57SOD1^{G93A} mice. Unlike skeletal muscle, the treatment modestly increased *Mcp1* levels in the sciatic nerves at 14 weeks (**Fig. 6A**). However, this did not further enhance the macrophages nor cytotoxic T cells recruitment, as demonstrated by the unchanged levels of *CD68* and *CD8a* transcripts than the scAAV9(empty)-treated group (**Fig. 6B, C**). In keeping with this, no difference in the *Tnfa* transcription was recorded in the sciatic nerve of SOD1^{G93A} mice compared with the NTg littermates (**Fig. 6D**).

At the symptomatic disease stage, the gene expression analysis showed a significant and similar upregulation of *Mcp1* and *CD68* transcripts in the PNS of both groups of SOD1^{G93A} mice compared with NTg littermates (**Fig. 6A, B**). Intriguingly, our analysis revealed a significant decrease in the CD68^{+} macrophages recruitment (**Fig. 6B**) and a reduction trend in the CD8^{+} lymphocytes infiltration (**Fig. 6C**) along motor axons of C57SOD1^{G93A} mice upon MCP1 boosting. The diminished leucocytes recall significantly abated the PNS inflammation in scAAV9_MCP1-treated mice, as demonstrated by the *Tnfa* downregulation compared with the control group (**Fig. 6D**). This effect translated into an increased expression of the p75-neurotrophin receptor (p75^{NTR}) within the sciatic nerves of scAAV9_MCP1-treated mice compared with controls (**Figure 6E, F**), suggesting increased motor axon regeneration and remyelination upon MCP1 boosting [17,102]. Suitably, whilst the heavy neurofilament (NF200) and myelin basic protein (MBP) levels were significantly downregulated in the PNS of symptomatic SOD1^{G93A} mice, their expression resulted unchanged in the scAAV9_MCP1-treated mice compared with the NTg littermates (**Fig. 6E, G, H**). Altogether, these observations suggest the almost complete maintenance of the axonal structure and myelin ensheathment of the sciatic nerve of symptomatic C57SOD1^{G93A} mice upon MCP1 boosting.

The MCP1 induction within spinal motor neurons of C57SOD1^{G93A} mice is protective by decreasing neuroinflammation

We showed that the scAAV9_GFP spreads retrogradely from the injected muscles alongside the motor unit of mSOD1 mice, finally transducing MN soma (**Supplementary Fig. 2**). Therefore, we analysed the effect of chemokine induction on the neurodegenerative signature of ALS.

The gene expression analysis confirmed a significant *Mcp1* upregulation in the lumbar spinal cord of scAAV9_MCP1-treated mice compared with the control group at 14 weeks (**Fig. 7D**). Conversely, at 20 weeks, no difference was recorded between the two groups of SOD1^{G93A} mice (**Fig. 7D**), suggesting that, at the full-blown stage, the massive chemokine expression by microglia ([103,104], **Fig. 1E**, **Supplementary Fig. 1C, F**) might mask the neuronal scAAV9-mediated induction.

Intriguingly, upon chemokine boosting, lumbar MNs resulted significantly spared from the degenerative phenomenon, even several weeks from the scAAV9_MCP1 injection (MN No. 14weeks: 4.3±0.06 Empty, 5.9±0.29 MCP1; 20 weeks: 2.1±0.22 Empty, 3.3±0.04 MCP1. mean±SEM) (**Fig. 7A-C**).

At 14 weeks, the anti-inflammatory markers Interleukin 4 (*Il4)* (**Fig. 7E**) and Arg1 (**Fig. 7G, H**) were significantly upregulated in the CNS of scAAV9_MCP1-treated mice; whereas, at the symptomatic disease stage, the treatment resulted in a significant downregulation of the pro-inflammatory factors Interleukin 1β (*Il1β*) (**Fig. 7F**) and gp91^{PHOX} (**Fig. 7G, I**) compared with the scAAV9(empty) group. These modifications did not alter the glia activation state, as demonstrated by the unchanged expression levels of the Ionised calcium-binding adapter molecule 1 (Iba1) and glial fibrillary acidic protein (GFAP) between the two groups of C57SOD1^{G93A} mice (**Supplementary Fig. 6A, B**). These data suggest that the MCP1 boosting in spinal MNs might have extended the so-called "stable phase" of the disease in SOD1^{G93A} mice [105,106], preserving the glia towards an anti-inflammatory phenotype followed later by the inhibition of pro-inflammatory environment, which reflected in MN preservation.

The MCP1 boosting in forelimb skeletal muscles of C57 SOD1^{G93A} mice delayed the denervation atrophy through immune-related myogenesis

The mSOD1 mice first develop hindlimb tremors, then progressive hindlimb weakness with rapidly deteriorating gait, eventually culminating in the paralysis of one or both hindlimbs [71,107–109]. Forelimbs function remains comparatively spared throughout the disease progression, indicating a distinct susceptibility of the upper motor unit in mSOD1 mice [57,71,110]. This evidence highlighted the importance of the forelimbs contribution in the disease progression of ALS mice, particularly at the advanced disease stage [57].

Likewise the hindlimbs, alterations in the forepaws could be detectable before evident motor impairment [67]. Accordingly, the muscle weight measurement showed that at 14 weeks the TB muscle of SOD1^{G93A} mice has already lost the 19.3±2.6% (mean±SEM) of its mass compared with the NTg littermates, which increased to 45.8±4.6% (mean±SEM) at 20 weeks. Notably, the MCP1 boosting significantly preserved the forepaw muscle of C57SOD1^{G93A} mice from the atrophic phenomenon reducing the muscle mass loss to 2.5±1.9% and 33.3±3.2%, respectively (mean±SEM) (**Fig. 8A**). Suitably, starting from the 14 weeks, our analysis showed a significant *AChRγ* upregulation in the TB muscle of SOD1^{G93A} mice, an effect magnified at 20 weeks corroborating the early and progressive NMJ alteration prior to the appearance of any sign of motor impairment. Notably, the MCP1 boosting remarkably prevented the NMJ denervation as demonstrated by the significant *AChRγ* downregulation compared with the scAAV9(empty)-treated mice at both time points (**Fig. 8B**).

As for the TA muscle, a single scAAV9_MCP1 i.m. injection resulted in a long-lasting *Mcp1* upregulation compared with the control groups and with the same extent at both the considered time points (**Fig. 8C**). Suitably, macrophages recruitment dramatically increased in the TB muscle of scAAV9_MCP1-treated mice compared with the control groups at 14 and 20 weeks (**Fig. 8D-F**). Besides, MCP1 boosting fostered the infiltration of cytotoxic CD8$^+$ T cells, but not CD4$^+$ T lymphocytes and FoxP3$^+$ Tregs, only at 14 weeks, suggesting an early inflammatory response within the forepaw muscle. Indeed, in the scAAV9(empty)-treated mice, a slightly heightened of T cells and Tregs infiltration was recorded only at the symptomatic disease stage (**Fig. 8G-I**).

This evidence was corroborated by the *Tnfa* upregulation recorded in the TB muscle of 14 weeks-old scAAV9_MCP1-treated mice compared with controls (**Fig. 9A**), and by the unchanged expression of Arg1 between the two groups of SOD1^{G93A} mice (**Fig. 9C, D**), suggesting a massive infiltration of M1-polarised leucocytes six weeks after the scAAV9_MCP1 injection. Notably, our analysis revealed a significant increase of *Igf1* transcript in the TB muscle of scAAV9_MCP1-treated mice (**Fig. 9B**), indicating the ongoing switching of infiltrated M1 cells towards the M2 pro-healing phenotype [81]. Accordingly, at 20 weeks, the *Tnfa* downregulation (**Fig. 9A**), the heightened Arg1 expression and the decreased *Igf1* transcription compared with controls (**Fig. 9B-D**) suggested the establishment of an anti-inflammatory muscular milieu twelve weeks after the scAAV9_MCP1 injection.

The histological analysis of transverse TB muscle sections showed that the MCP1-mediated immune cells infiltration did not significantly modify the quiescent status of the SCs at the pre-symptomatic disease stage (**Supplementary Fig. 7A, C**). Accordingly, no significant difference in the percentage of centralised myonuclei was recorded between the two groups of SOD1^{G93A} mice at 14 weeks, albeit an increasing trend was noticeable upon MCP1 boosting (**Supplementary Fig. 7B, D**). Conversely, at 20 weeks, the switch of the recruited leucocytes towards the M2 pro-healing phenotype promoted the TB regeneration in scAAV9_MCP1-treated mice, as demonstrated by the increased percentage of differentiating Pax7^{-}/MyoD^{+} SCs (Empty: 10.5±3.6%; MCP1: 19.5±2.3%. mean±SEM) (**Fig. 9E-G**) and centralised myonuclei (% Vs Ntg: 155.6±28.2, Empty; 234.8±31.8, MCP1. mean±SEM) compared with the control group (**Fig. 9F, H**).

The MCP1 induction in 129SvSOD1^{G93A} mice exacerbated inflammation in the periphery worsening the clinical phenotype

The data collected demonstrated the beneficial action of MCP1 within the motor unit of C57SOD1^{G93A} mice. Therefore, we assessed whether the chemokine induction in 129SvSOD1^{G93A} mice, which show a faint activation of the MCP1 axis, was able to ameliorate the disease progression.

Eight-week-old 129SvSOD1^{G93A} mice (No.12 per group) were i.m. injected with the scAAV9_MCP1 and monitored until the clear symptomatic disease stage (17 weeks). The behavioural analysis showed that neither the bodyweight nor the motor onset was modified by the chemokine boosting (Empty, 14.1±0.4 weeks; MCP1, 13.4±0.4 weeks. mean±SEM) (**Fig. 10 A, C**). Nevertheless, a worsening of the grip strength impairment was recorded in the scAAV9_MCP1-treated mice at the advanced disease stages (**Fig. 10B**). However, the histological examination did not reveal any difference between the two groups of 129SvSOD1^{G93A} mice in the extent of NMJ denervation and TA muscle atrophy (**Fig. 10D-F**).

Compared to C57SOD1^{G93A} mice, at the symptomatic disease stage, fast-progressing mSOD1 mice strongly upregulated the chemokine within the TA muscle compared to respective Ntg littermates (FC = 65.1±12.4, 129SvSOD1^{G93A} mice; FC = 3±0.2, C57SOD1^{G93A} mice. mean±SEM), which dramatically increased upon scAAV9_MCP1 injection (FC = 752.1±208.4. mean±SEM) (**Fig. 10G**). Interestingly, the analysis of CD68^{+} cells density and *CD8a* and *CD4* transcripts demonstrated massive recruitment of

macrophages and T lymphocytes in the hind paw muscle of scAAV9_MCP1- but not scAAV9(empty)-treated group compared with the NTg littermates (**Fig. 10H-K**), suggesting a drastic alteration of the muscular inflammatory response in 129SvSOD1^{G93A} mice upon chemokine boosting. Notwithstanding the significant *Foxp3* upregulation (**Fig. 10L**), an intense inflammation characterised the TA muscle of scAAV9_MCP1-treated mice, arguably due to the impaired immunomodulatory capability of Tregs of mSOD1 mice at the advanced disease stage [106]. Accordingly, the pro-inflammatory markers *Tnfa* and gp91^{PHOX} were significantly upregulated in scAAV9_MCP1-treated mice (**Supplementary Fig. 8A, C, D**). Conversely, the expression level of the anti-inflammatory factor Arg1 was unchanged between the two groups of 129SvSOD1^{G93A} mice, whereas the *Igf1* was downregulated, indicating that the infiltrated M1-macrophages (**Supplementary Fig. 8A, B**) were not apt to switch towards the M2 pro-healing phenotype [81] (**Supplementary Fig. 8E**). Besides, the MCP1 boosting was unable to upregulate further the Pax7 and MyoG expression in 129SvSOD1^{G93A} mice (**Supplementary Fig. 8A, F, G**), suggesting a worthless myogenic response by mSOD1 mice at the advanced disease stage.

Since in C57SOD1^{G93A} scAAV9_MCP1-treated mice the chemokine-mediated protective role arose early in the disease course, we assessed the effect of MCP1 boosting in fast-progressing mSOD1 mice ~2 weeks before the motor symptoms appearance. Six-week-old 129SvSOD1^{G93A} mice (5 per group) were i.m. injected with the scAAV9 vectors, and the analysis of TA muscle was performed at 12 weeks of age. Intriguingly, although *Mcp1* resulted markedly upregulated (**Supplementary Fig. 9C**), 129SvSOD1^{G93A} mice appeared insensitive to the chemokine boosting as demonstrated by the unchanged CD68^{+} macrophages recruitment compared with the scAAV9(empty) group (**Supplementary Fig. 9A, B**). Indeed, no difference in the extent of the TA muscle atrophy was recorded between the two groups of 129SvSOD1^{G93A} mice at 12 weeks (**Supplementary Fig. 9D**).

Altogether, the data collected indicate a laggard activation of the muscular immune response by fast-progressing SOD1^{G93A} mice, culminating in an exacerbated inflammation upon MCP1 boosting that might be responsible for the worsened clinical phenotype at the advanced disease stage.

Discussion

In this study, we examined the involvement of the MCP1-mediated axis in governing the speed of ALS progression in two SOD1^{G93A} models characterised by remarkable differences in the disease progression rate.

Our observations revealed that, albeit the scAAV9_MCP1 i.m. injection boosted the chemokine to the same extent along the neuromuscular system of the two ALS models, the treatment led to an opposite effect on the clinical phenotype of C57 compared with 129Sv mSOD1 mice. Slow-progressing C57SOD1^{G93A} mice responded positively to MCP1 boosting, anticipating the recruitment and phenotypic switch of leucocytes within the peripheral compartment. This sustained the activation of the myogenic programme and nerve regeneration, finally slackening off the motor symptoms. Conversely, fast-

progressing 129SvSOD1^{G93A} mice exhibited an adverse response to the treatment, exacerbating the toxic inflammatory response in the periphery, resulting in worsened motor ability late in the disease.

Intriguingly, our data showed a novel immune-unrelated role for MCP1 in promoting motor axon regeneration and modulating neuroinflammation in the nervous system of mSOD1 mice, with the overall effect of slackening MN degeneration.

We recently reported a different activation of MCP1 within MN soma and peripheral compartment of fast-*versus* slow-progressing SOD1^{G93A} models [26,28]. Our studies revealed that fast-progressing mSOD1 mice exhibited earlier muscle denervation and motor axon deterioration correlated with lower immune cells infiltration in the peripheral compartment than slow-progressing mSOD1 mice [26,27]. We speculated that this defective immune response underpinned the greater peripheral degeneration and more rapid disease course of 129SvSOD1^{G93A} mice. This evidence put the MCP1-mediated immune cell recruitment forward as a discriminating factor of the different speed in the disease progression of the two mSOD1 models.

MCP1 is a chemokine with a renowned pro-inflammatory capability [111]. In the neurological context, the increased expression of MCP1 is usually associated with neurodegenerative/neuroinflammatory diseases [112–114], including ALS [115–117]. Accordingly, in the spinal cord of SOD1^{G93A} mice, we recorded a gradual increase of MCP1 levels as the disease progresses, characterised by a strong expression by microglia at the advanced disease stage.

Besides its classic toxic inflammatory activity, several evidence indicated a pivotal role of the MCP1-mediated axis at orchestrating nerve [118–121] and muscle [29,49,79,122] regeneration. In keeping with this, we recorded a gradual increase of chemokine expression along motor axons and Schwann cells as the disease progresses, suggesting the protective role of MCP1 in the PNS of mSOD1 mice.

Immune cells infiltration has been reported within nerves and skeletal muscles in ALS [16,54,55,123,124], albeit its contribution to the disease progression is still elusive. Here we assessed the influence of peripheral immune response in fast- and slow-progressing SOD1^{G93A} mice through the i.m. injection of scAAV9_MCP1, which neatly boosted the chemokine along the motor unit of both ALS models.

The data herein collected highlighted a delayed activation of the immune response in the muscular compartment of mSOD1 mice. Indeed, at 14 weeks (i.e. ~2 weeks before the overt muscle strength impairment), in concomitance with a pronounced TA muscle denervation atrophy, C57SOD1^{G93A} mice have just launched the inflammatory response activating resident macrophages and recruiting neutrophils, which are the first immune cells entering within the damage site to amplify the inflammation and promote the recruitment of haematogenous leucocytes [89,90]. Conversely, the early MCP1 boosting anticipated the inflammatory response within the muscular compartment of slow-progressing mSOD1 mice. Indeed, a “second wave” of immune cell infiltration, in which neutrophils gave way to macrophages and T lymphocytes [53,85,86], characterised the TA muscle of C57SOD1^{G93A} mice six weeks after the

scAAV9_MCP1 injection. Intriguingly, our analysis revealed that the immunosuppressive capability of MCP1-recruited Tregs [125] dampened the inflammation within the damaged tissue, sustaining the switch of M1 phagocytic macrophages towards the M2 pro-regenerative phenotype [88,126,127]. In keeping with the *Tnfa* and *Igf1* downregulation and increased Sirt1 expression [81,82], a higher percentage of $CD206^{+}$ M2-macrophages was recorded in the TA muscle of scAAV9_MCP1-treated mice compared with the scAAV9(empty) group, which got stuck on the “first wave” of the immune response [53,85,86].

The anticipated peripheral immune response of scAAV9_MCP1-treated C57$SOD1^{G93A}$ mice reflected into increased myogenic activity by virtue of the lack of the inhibitory action of neutrophils [128] and inductive action of the Tregs and M2 macrophages on myogenic progenitor cells [85,87,91,129]. This translated into TA muscle regeneration and preservation from denervation atrophy and metabolic dysregulation compared with the control group.

The same extent of TA muscle atrophy registered in scAAV9_MCP1- and scAAV9(empty)-treated mice at 20 weeks indicated gradual exhaustion of the elicited muscle pro-healing immune response in the hindlimbs of C57$SOD1^{G93A}$ mice as the disease progresses. However, the preservation of the forepaw muscles, which are belatedly affected in the mSOD1 model [71,109,110], might be partially responsible for the ameliorated motor performance of slow-progressing mSOD1 scAAV9_MCP1-treated mice at the advanced disease stage [57]. The early MCP1 boosting within TB muscle of C57$SOD1^{G93A}$ mice forced and sustained the pro-inflammatory response at 14 weeks, which was decisive at countenancing its transition towards the anti-inflammatory and pro-regenerative state [50,130], eventually preventing the forepaw muscle denervation atrophy at the symptomatic disease stage.

The evidence herein collected highlighted the pivotal role of the peripheral immune response in triggering skeletal muscle regeneration and its temporal activation as a limiting factor in achieving a significant effect to slacken off the disease progression in mSOD1 mice.

The delayed activation of the peripheral immune response was exacerbated in fast-progressing $SOD1^{G93A}$ mice, whose genetic background is associated with a poor ability at recruiting immune cells during phlogosis [131,132]. Accordingly, although the chemokine resulted massively upregulated six weeks after the scAAV9_MCP1 injection, 129Sv$SOD1^{G93A}$ mice were unable to promptly and properly react to the chemotactic gradient established within the TA muscle fostering the haematogenous macrophage recruitment. The deficient activation of the immune response early in the disease led to its mismanagement at the advanced stage. Indeed, pursuant to the dramatic macrophages and T lymphocytes recruitment, a massive and persistent inflammation characterised the TA muscle of 129Sv$SOD1^{G93A}$ scAAV9_MCP1-treated mice at 17 weeks, finally hampering skeletal muscle regeneration and function [53,130]. This result mirrored the recent findings by Rizzo et al. [133], who demonstrated that, in splenectomised *mdx* mice, the delayed macrophage infiltration impaired their shift towards the M2 pro-healing fingerprint, eventually hindering muscle fibres regeneration. Therefore, we can surmise that the tardive and maladaptive activation of the peripheral immune response, even upon MCP1 boosting, might be the chief culprit of faster disease progression of 129Sv$SOD1^{G93A}$ mice.

The data collected in the hind paw muscle of mSOD1 mice suggested that preserving the muscular compartment since the early disease stage might have slackened off ALS dying-back degeneration of the motor system [11]. Nevertheless, we demonstrated that the retrograde overexpression of MCP1 within the sciatic nerves of mSOD1 mice directly affected the stability and regeneration of peripheral motor axons. Indeed, the chemokine upregulation within the sciatic nerves of C57SOD1^{G93A} scAAV9_MCP1-treated mice resulted in increased sprouting of GAP43^{+} motor axon terminal branches, accounting for the reduced denervation atrophy of hindlimb muscles across the disease progression.

The MCP1 dispensable capability to promote axonal outgrowth was previously described in aSMN1-expressing NSC34 cells cultures [44] and DRG explants obtained from MCP1-treated [120,134] or genetically depleted mice [119]. According to this information, the chemokine plays an immune-unrelated role in amplifying and maintaining the regenerative capacity of peripheral axons, promoting the expression of the regeneration-associated genes (e.g. GAP43), which is concurrent to the MCP1-mediated neuron-macrophage interaction [45,119,134].

Based on our evidence, the MCP1 pro-regenerative effect in the PNS of mSOD1 mice became clear at the symptomatic disease stage when the chemokine overexpression preserved the motor axon cytoarchitecture and myelination, decreased toxic inflammation and sustained the collateral innervation of hindlimb skeletal muscles.

Albeit the MCP1 pleiotropic mechanism is far from being elucidated, recent studies reported the direct influence of the chemokine at modulating the neuroinflammation by governing the recruited myeloid cells fingerprint. For instance, several observations obtained in animal models of spinal cord injury demonstrated that MCP1 released by neurons attracts and activates macrophages through CCR2 to drive them toward the M2 pro-healing phenotype. In turn, MCP1-activated macrophages establish a permissive environment [119,134], eventually preventing neurodegeneration [45]. Here we showed that a similar mechanism could be prompted within the spinal cord of SOD1^{G93A} mice where MCP1 resulted significantly upregulated by MNs at the disease onset. Albeit it is now clear that haematogenous monocytes cannot penetrate the CNS of mSOD1 mice [16,135,136], we can suppose that the scAAV9-specific induction of MCP1 within MN perikaryon might have modulated the activation state of the CNS-resident myeloid cells (i.e. microglia). Suitably, our data demonstrated that the scAAV9_MCP1 injection in pre-symptomatic mSOD1 mice extended the so-called “stable phase” of the disease [105,106], maintaining the M2 polarisation of the neuroinflammatory milieu and reducing MN loss along the disease course.

Conclusions

For the first time in the ALS context, we demonstrated the pivotal role of the immune response in promoting and governing skeletal muscle regeneration and thus the speed of the disease progression. Our observations suggest that, although potentially protective, the immune response is delayed in ALS mice and, hence, ineffective at sustaining a substantial recovery of the peripheral compartment. Notably,

the dichotomic effect recorded in the two SOD1^{G93A} strains following MCP1 boosting pointed out the nature and temporal activation of the immune response as discriminating factors to foster skeletal muscle regeneration, slacken the dying-back degeneration and slow down ALS course. This also emphasizes the different immune response due to genetic background as a key determinant of the variability in the disease progression as reported in ALS patients carrying the same SOD1 mutation [3,4]. Altogether, these observations nominate the muscular compartment as a primary target for developing effective therapeutic interventions in ALS capable of interfering with the speed of the symptoms progression and the dying-back degeneration tangibly. Besides, the comprehension of the mechanisms underlying the protective role fulfil from MCP1 in the motor unit of mSOD1 mice might provide innovative evidence regarding the contribution of the immune response in ALS.

Despite *in vitro* and *in vivo* models of the disease have generated different potential pharmacological targets, ALS still lacks an adequate therapy able to delay or even halt its development [137,138]. We think that this is mainly due to the poor knowledge of the temporal and spatial mechanisms by which the immune response governs the pattern of the disease [139,140]. Our findings provide a possible explanation for the failure of unspecific immunomodulatory treatments [23,141] and suggest new potential strategies to prevent ALS progression.

Altogether, the evidence herein provided demonstrated the crucial role of the so-far-underestimated peripheral compartment in ALS pathoprogression straightforwardly. Although the latest clinical studies reported a defective monocyte/macrophages infiltration at the site of nerve degeneration [142] and a direct correlation between the PNS inflammation and longer disease duration [21], no observations are still available on the first body compartment affected by ALS: the skeletal muscle. Therefore, in virtue of the easy accessibility of bioptic samples, the characterisation of the immune muscle fingerprint to assess a potential correlation with biomolecular pathways underlying atrophy and myogenesis might produce a combination of muscle-derived, immune-related molecular signatures that will be useful as a clinical adjunct in the prognostic evaluation of ALS patients.

Abbreviations

MCP1: Monocyte Chemoattractant Protein 1; MN: motor neuron; mSOD1: mutant Superoxide Dismutase 1; SC: satellite cell; TB: Triceps Brachii; TA: Tibialis Anterior; scAAV9: self-complementary Adeno-Associated Virus

Declarations

Acknowledgements

Not applicable

Funding

This work was supported by the Fondazione Italiana di Ricerca per la Sclerosi Laterale Amiotrofica (AriSLA Grant “MacrophALS” and “IMMUNALS”), and the “Translating molecular mechanisms into ALS risk and patient’s well- being” (TRANSALS) - Regione Lombardia (no. 2015-0023).

Availability of data and materials

The authors confirm that the data, materials, and software information supporting the findings of this study are available within the article and its supplementary materials.

Authors’ contributions

MCT treated mSOD1 mice. Besides, she collected mouse tissues, analysed the behavioural data, did the immunohistochemical (IHC), biomolecular, and biochemical analysis with the help of PF, VM, CS and FS under the supervision of GN. CS and VM were the blind operators in the behavioural and IHC/biochemical analysis under the supervision of MCT. MR did the immunohistochemical analysis of MCP1 expression in the nervous system under the supervision of GN. GN and MCT designed the experiments under the supervision of CB. MCT, GN and CB wrote the manuscript. All authors have read and approved the final version of the manuscript.

Ethics approval and consent to participate

All procedures performed in studies involving animals were in accordance with the ethical standards of the Mario Negri Institute at which the studies were conducted**.**

Consent for publication

The corresponding authors have obtained informed consent from all participants in the study.

Competing interests

The authors declare that they have no competing interests.

References

1. Hardiman O, Al-Chalabi A, Chio A, Corr EM, Logroscino G, Robberecht W, et al. Amyotrophic lateral sclerosis. Nat Rev Dis Prim [Internet]. 2017;3:17071. Available from: http://www.ncbi.nlm.nih.gov/pubmed/28980624

2. Masrori P, Van Damme P. Amyotrophic lateral sclerosis: a clinical review. Eur J Neurol [Internet]. 2020;27:1918–29. Available from: https://onlinelibrary.wiley.com/doi/10.1111/ene.14393

3. Penco S, Lunetta C, Mosca L, Maestri E, Avemaria F, Tarlarini C, et al. Phenotypic heterogeneity in a SOD1 G93D Italian ALS family: an example of human model to study a complex disease. J Mol Neurosci [Internet]. 2011;44:25–30. Available from: http://www.ncbi.nlm.nih.gov/pubmed/21120636

4. Régal L, Vanopdenbosch L, Tilkin P, Van den Bosch L, Thijs V, Sciot R, et al. The G93C mutation in superoxide dismutase 1: clinicopathologic phenotype and prognosis. Arch Neurol [Internet]. 2006;63:262–7. Available from: http://www.ncbi.nlm.nih.gov/pubmed/16476815

5. Ticozzi N, Silani V. Genotypic and Phenotypic Heterogeneity in Amyotrophic Lateral Sclerosis. Neurodegener Dis [Internet]. Cham: Springer International Publishing; 2018. p. 279–95. Available from: http://link.springer.com/10.1007/978-3-319-72938-1_13

6. Bendotti C, Bonetto V, Pupillo E, Logroscino G, Al-Chalabi A, Lunetta C, et al. Focus on the heterogeneity of amyotrophic lateral sclerosis. Amyotroph Lateral Scler Frontotemporal Degener [Internet]. 2020;1–11. Available from: http://www.ncbi.nlm.nih.gov/pubmed/32583689

7. Mejzini R, Flynn LL, Pitout IL, Fletcher S, Wilton SD, Akkari PA. ALS Genetics, Mechanisms, and Therapeutics: Where Are We Now? Front Neurosci. 2019;13:1–27.

8. Rouaux C, Panteleeva I, René F, Gonzalez de Aguilar J-L, Echaniz-Laguna A, Dupuis L, et al. Sodium valproate exerts neuroprotective effects in vivo through CREB-binding protein-dependent mechanisms but does not improve survival in an amyotrophic lateral sclerosis mouse model. J Neurosci [Internet]. 2007;27:5535–45. Available from: http://www.ncbi.nlm.nih.gov/pubmed/17522299

9. Gould TW, Buss RR, Vinsant S, Prevette D, Sun W, Knudson CM, et al. Complete dissociation of motor neuron death from motor dysfunction by Bax deletion in a mouse model of ALS. J Neurosci [Internet]. 2006;26:8774–86. Available from: http://www.ncbi.nlm.nih.gov/pubmed/16928866

10. Moloney EB, de Winter F, Verhaagen J. ALS as a distal axonopathy: molecular mechanisms affecting neuromuscular junction stability in the presymptomatic stages of the disease. Front Neurosci [Internet]. 2014;8:252. Available from: http://www.ncbi.nlm.nih.gov/pubmed/25177267

11. Dadon-Nachum M, Melamed E, Offen D. The “dying-back” phenomenon of motor neurons in ALS. J Mol Neurosci. 2011;43:470–7.

12. Gentile F, Scarlino S, Falzone YM, Lunetta C, Tremolizzo L, Quattrini A, et al. The peripheral nervous system in amyotrophic lateral sclerosis: Opportunities for translational research. Front Neurosci. 2019;13:1–16.

13. Chiot A, Lobsiger CS, Boillée S. New insights on the disease contribution of neuroinflammation in amyotrophic lateral sclerosis. Curr Opin Neurol [Internet]. 2019;32:764–70. Available from: http://www.ncbi.nlm.nih.gov/pubmed/31306211

14. Thonhoff JR, Simpson EP, Appel SH. Neuroinflammatory mechanisms in amyotrophic lateral sclerosis pathogenesis. Curr Opin Neurol [Internet]. 2018;31:635–9. Available from: http://www.ncbi.nlm.nih.gov/pubmed/30048339

15. Dibaj P, Steffens H, Zschüntzsch J, Nadrigny F, Schomburg ED, Kirchhoff F, et al. In Vivo imaging reveals distinct inflammatory activity of CNS microglia versus PNS macrophages in a mouse model for ALS. PLoS One [Internet]. 2011;6:e17910. Available from: http://www.ncbi.nlm.nih.gov/pubmed/21437247

16. Chiu IM, Phatnani H, Kuligowski M, Tapia JC, Carrasco MA, Zhang M, et al. Activation of innate and humoral immunity in the peripheral nervous system of ALS transgenic mice. Proc Natl Acad Sci U S A. 2009;106:20960–5.

17. Deng B, Lv W, Duan W, Liu Y, Li Z, Ma Y, et al. Progressive Degeneration and Inhibition of Peripheral Nerve Regeneration in the SOD1-G93A Mouse Model of Amyotrophic Lateral Sclerosis. Cell Physiol Biochem [Internet]. 2018;46:2358–72. Available from: http://www.ncbi.nlm.nih.gov/pubmed/29742495

18. Van Dyke JM, Smit-Oistad IM, Macrander C, Krakora D, Meyer MG, Suzuki M. Macrophage-mediated inflammation and glial response in the skeletal muscle of a rat model of familial amyotrophic lateral sclerosis (ALS). Exp Neurol [Internet]. 2016;277:275–82. Available from: http://www.ncbi.nlm.nih.gov/pubmed/26775178

19. Gaudet AD, Popovich PG, Ramer MS. Wallerian degeneration: Gaining perspective on inflammatory events after peripheral nerve injury [Internet]. J. Neuroinflammation. 2011 [cited 2019 Sep 17]. p. 110. Available from: http://jneuroinflammation.biomedcentral.com/articles/10.1186/1742-2094-8-110

20. Sass FA, Fuchs M, Pumberger M, Geissler S, Duda GN, Perka C, et al. Immunology Guides Skeletal Muscle Regeneration. Int J Mol Sci [Internet]. 2018;19. Available from: http://www.ncbi.nlm.nih.gov/pubmed/29534011

21. Schreiber S, Schreiber F, Garz C, Debska-Vielhaber G, Assmann A, Perosa V, et al. Toward in vivo determination of peripheral nervous system immune activity in amyotrophic lateral sclerosis. Muscle Nerve [Internet]. 2019;59:567–76. Available from: http://www.ncbi.nlm.nih.gov/pubmed/30734322

22. Lyon MS, Wosiski-Kuhn M, Gillespie R, Caress J, Milligan C. Inflammation, Immunity, and amyotrophic lateral sclerosis: I. Etiology and pathology. Muscle and Nerve [Internet]. John Wiley & Sons, Ltd; 2019;59:10–22. Available from: http://doi.wiley.com/10.1002/mus.26289

23. Wosiski-Kuhn M, Lyon MS, Caress J, Milligan C. Inflammation, immunity, and amyotrophic lateral sclerosis: II. immune-modulating therapies. Muscle Nerve [Internet]. 2019 [cited 2019 Sep 19];59:23–33. Available from: http://doi.wiley.com/10.1002/mus.26288

24. Marino M, Papa S, Crippa V, Nardo G, Peviani M, Cheroni C, et al. Differences in protein quality control correlate with phenotype variability in 2 mouse models of familial amyotrophic lateral sclerosis. Neurobiol Aging [Internet]. 2015;36:492–504. Available from: https://linkinghub.elsevier.com/retrieve/pii/S0197458014004655

25. Nardo G, Trolese MCMC, Tortarolo M, Vallarola A, Freschi M, Pasetto L, et al. New Insights on the Mechanisms of Disease Course Variability in ALS from Mutant SOD1 Mouse Models. Brain Pathol [Internet]. 2016;26:237–47. Available from: http://www.ncbi.nlm.nih.gov/pubmed/26780365

26. Nardo G, Trolese MC, de Vito G, Cecchi R, Riva N, Dina G, et al. Immune response in peripheral axons delays disease progression in SOD1G93A mice. J Neuroinflammation [Internet]. 2016;13:261. Available from: http://www.ncbi.nlm.nih.gov/pubmed/27717377

27. Vallarola A, Sironi F, Tortarolo M, Gatto N, De Gioia R, Pasetto L, et al. RNS60 exerts therapeutic effects in the SOD1 ALS mouse model through protective glia and peripheral nerve rescue. J Neuroinflammation [Internet]. 2018;15:65. Available from: http://www.ncbi.nlm.nih.gov/pubmed/29495962

28. Nardo G, Iennaco R, Fusi N, Heath PR, Marino M, Trolese MC, et al. Transcriptomic indices of fast and slow disease progression in two mouse models of amyotrophic lateral sclerosis. Brain [Internet]. 2013;136:3305–32. Available from: http://www.ncbi.nlm.nih.gov/pubmed/24065725

29. Shireman PK, Contreras-Shannon V, Ochoa O, Karia BP, Michalek JE, McManus LM. MCP-1 deficiency causes altered inflammation with impaired skeletal muscle regeneration. J Leukoc Biol. 2007;81:775–85.

30. Siebert H, Sachse A, Kuziel WA, Maeda N, Brück W. The chemokine receptor CCR2 is involved in macrophage recruitment to the injured peripheral nervous system. J Neuroimmunol [Internet]. 2000;110:177–85. Available from: http://www.ncbi.nlm.nih.gov/pubmed/11024548

31. Han KH, Tangirala RK, Green SR, Quehenberger O. Chemokine receptor CCR2 expression and monocyte chemoattractant protein-1-mediated chemotaxis in human monocytes. A regulatory role for plasma LDL. Arterioscler Thromb Vasc Biol [Internet]. 1998;18:1983–91. Available from: http://www.ncbi.nlm.nih.gov/pubmed/9848893

32. Gendelman HE, Ding S, Gong N, Liu J, Ramirez SH, Persidsky Y, et al. Monocyte chemotactic protein-1 regulates voltage-gated K+ channels and macrophage transmigration. J Neuroimmune Pharmacol [Internet]. 2009;4:47–59. Available from: http://www.ncbi.nlm.nih.gov/pubmed/19034671

33. He M, Dong H, Huang Y, Lu S, Zhang S, Qian Y, et al. Astrocyte-Derived CCL2 is Associated with M1 Activation and Recruitment of Cultured Microglial Cells. Cell Physiol Biochem [Internet]. 2016;38:859–70. Available from: https://www.karger.com/Article/FullText/443040

34. Carr MW, Roth SJ, Luther E, Rose SS, Springer TA. Monocyte chemoattractant protein 1 acts as a T-lymphocyte chemoattractant. Proc Natl Acad Sci U S A [Internet]. 1994;91:3652–6. Available from: http://www.ncbi.nlm.nih.gov/pubmed/8170963

35. Frade JM, Mellado M, del Real G, Gutierrez-Ramos JC, Lind P, Martinez-A C. Characterization of the CCR2 chemokine receptor: functional CCR2 receptor expression in B cells. J Immunol [Internet].

1997;159:5576–84. Available from: http://www.ncbi.nlm.nih.gov/pubmed/9548499

36. Allavena P, Bianchi G, Zhou D, van Damme J, Jílek P, Sozzani S, et al. Induction of natural killer cell migration by monocyte chemotactic protein-1, -2 and -3. Eur J Immunol [Internet]. 1994;24:3233–6. Available from: http://www.ncbi.nlm.nih.gov/pubmed/7805752

37. Xu P, Zhang J, Wang H, Wang G, Wang C-Y, Zhang J. CCR2 dependent neutrophil activation and mobilization rely on TLR4-p38 axis during liver ischemia-reperfusion injury. Am J Transl Res [Internet]. 2017;9:2878–90. Available from: http://www.ncbi.nlm.nih.gov/pubmed/28670376

38. Semple BD, Kossmann T, Morganti-Kossmann MC. Role of chemokines in CNS health and pathology: a focus on the CCL2/CCR2 and CXCL8/CXCR2 networks. J Cereb Blood Flow Metab [Internet]. 2010;30:459–73. Available from: http://www.ncbi.nlm.nih.gov/pubmed/19904283

39. Martínez HRR, Escamilla-Ocañas CEE, Camara-Lemarroy CRR, González-Garza MTT, Moreno-Cuevas J, García Sarreón MAA. Increased cerebrospinal fluid levels of cytokines monocyte chemoattractant protein-1 (MCP-1) and macrophage inflammatory protein-1β (MIP-1β) in patients with amyotrophic lateral sclerosis. Neurologia [Internet]. 2020;35:165–9. Available from: https://linkinghub.elsevier.com/retrieve/pii/S217358082030050X

40. Henkel JS, Beers DR, Siklós L, Appel SH. The chemokine MCP-1 and the dendritic and myeloid cells it attracts are increased in the mSOD1 mouse model of ALS. Mol Cell Neurosci [Internet]. 2006;31:427–37. Available from: http://www.ncbi.nlm.nih.gov/pubmed/16337133

41. Dzenko KA, Song L, Ge S, Kuziel WA, Pachter JS. CCR2 expression by brain microvascular endothelial cells is critical for macrophage transendothelial migration in response to CCL2. Microvasc Res [Internet]. 2005;70:53–64. Available from: http://www.ncbi.nlm.nih.gov/pubmed/15927208

42. Chintawar S, Cayrol R, Antel J, Pandolfo M, Prat A. Blood-brain barrier promotes differentiation of human fetal neural precursor cells. Stem Cells [Internet]. 2009;27:838–46. Available from: http://www.ncbi.nlm.nih.gov/pubmed/19350685

43. Liu XS, Zhang ZG, Zhang RL, Gregg SR, Wang L, Yier T, et al. Chemokine ligand 2 (CCL2) induces migration and differentiation of subventricular zone cells after stroke. J Neurosci Res [Internet]. 2007;85:2120–5. Available from: http://www.ncbi.nlm.nih.gov/pubmed/17510981

44. Locatelli D, Terao M, Fratelli M, Zanetti A, Kurosaki M, Lupi M, et al. Human axonal Survival of Motor Neuron (a-SMN) protein stimulates axon growth, cell motility, C-C motif ligand 2 (CCL2),andinsulin-like growth factor-1 (IGF1) production. J Biol Chem [Internet]. 2012 [cited 2019 Sep 17];287:25782–94. Available from: http://www.jbc.org/lookup/doi/10.1074/jbc.M112.362830

45. Papa S, Vismara I, Mariani A, Barilani M, Rimondo S, De Paola M, et al. Mesenchymal stem cells encapsulated into biomimetic hydrogel scaffold gradually release CCL2 chemokine in situ preserving

cytoarchitecture and promoting functional recovery in spinal cord injury. J Control Release [Internet]. 2018;278:49–56. Available from: https://linkinghub.elsevier.com/retrieve/pii/S0168365918301731

46. Liu P, Peng J, Han GH, Ding X, Wei S, Gao G, et al. Role of macrophages in peripheral nerve injury and repair. Neural Regen Res. 2019;14:1335–42.

47. Chen P, Piao X, Bonaldo P. Role of macrophages in Wallerian degeneration and axonal regeneration after peripheral nerve injury. Acta Neuropathol. Springer Berlin Heidelberg; 2015;130:605–18.

48. Zigmond RE, Echevarria FD. Macrophage biology in the peripheral nervous system after injury. Prog Neurobiol [Internet]. Elsevier; 2019;173:102–21. Available from: https://doi.org/10.1016/j.pneurobio.2018.12.001

49. Martinez CO, McHale MJ, Wells JT, Ochoa O, Michalek JE, McManus LM, et al. Regulation of skeletal muscle regeneration by CCR2-activating chemokines is directly related to macrophage recruitment. Am J Physiol - Regul Integr Comp Physiol [Internet]. 2010;299:R832-42. Available from: https://www.physiology.org/doi/10.1152/ajpregu.00797.2009

50. Dort J, Fabre P, Molina T, Dumont NA. Macrophages Are Key Regulators of Stem Cells during Skeletal Muscle Regeneration and Diseases. Stem Cells Int [Internet]. 2019;2019:1–20. Available from: https://www.hindawi.com/journals/sci/2019/4761427/

51. Zhang J, Xiao Z, Qu C, Cui W, Wang X, Du J. CD8 T Cells Are Involved in Skeletal Muscle Regeneration through Facilitating MCP-1 Secretion and Gr1 high Macrophage Infiltration. J Immunol [Internet]. 2014;193:5149–60. Available from: http://www.jimmunol.org/lookup/doi/10.4049/jimmunol.1303486

52. Deyhle MR, Hyldahl RD. The Role of T Lymphocytes in Skeletal Muscle Repair From Traumatic and Contraction-Induced Injury. Front Physiol [Internet]. 2018;9:768. Available from: http://www.ncbi.nlm.nih.gov/pubmed/29973887

53. Yang W, Hu P. Skeletal muscle regeneration is modulated by inflammation. J Orthop Transl [Internet]. 2018;13:25–32. Available from: https://linkinghub.elsevier.com/retrieve/pii/S2214031X17300621

54. Kano O, Beers DR, Henkel JS, Appel SH. Peripheral nerve inflammation in ALS mice: cause or consequence. Neurology [Internet]. 2012;78:833–5. Available from: http://www.neurology.org/cgi/doi/10.1212/WNL.0b013e318249f776

55. Trias E, King PH, Si Y, Kwon Y, Varela V, Ibarburu S, et al. Mast cells and neutrophils mediate peripheral motor pathway degeneration in ALS. JCI Insight [Internet]. 2018;3. Available from: https://insight.jci.org/articles/view/123249

56. Gruntman AM, Bish LT, Mueller C, Sweeney HL, Flotte TR, Gao G. Gene transfer in skeletal and cardiac muscle using recombinant adeno-associated virus. Curr Protoc Microbiol [Internet]. 2013;Chapter 14:Unit 14D.3. Available from: http://www.ncbi.nlm.nih.gov/pubmed/23408131

57. Nardo G, Trolese MC, Verderio M, Mariani A, de Paola M, Riva N, et al. Counteracting roles of MHCI and CD8+ T cells in the peripheral and central nervous system of ALS SOD1G93A mice. Mol Neurodegener [Internet]. 2018;13:42. Available from: http://www.ncbi.nlm.nih.gov/pubmed/30092791

58. Lauranzano E, Pozzi S, Pasetto L, Stucchi R, Massignan T, Paolella K, et al. Peptidylprolyl isomerase A governs TARDBP function and assembly in heterogeneous nuclear ribonucleoprotein complexes. Brain [Internet]. 2015;138:974–91. Available from: http://www.ncbi.nlm.nih.gov/pubmed/25678563

59. Friese A, Kaltschmidt JA, Ladle DR, Sigrist M, Jessell TM, Arber S. Gamma and alpha motor neurons distinguished by expression of transcription factor Err3. Proc Natl Acad Sci U S A [Internet]. 2009;106:13588–93. Available from: http://www.ncbi.nlm.nih.gov/pubmed/19651609

60. Geuna S, Tos P, Guglielmone R, Battiston B, Giacobini-Robecchi MG. Methodological issues in size estimation of myelinated nerve fibers in peripheral nerves. Anat Embryol (Berl) [Internet]. 2001;204:1–10. Available from: http://www.ncbi.nlm.nih.gov/pubmed/11506429

61. Mayeuf-Louchart A, Hardy D, Thorel Q, Roux P, Gueniot L, Briand D, et al. MuscleJ: a high-content analysis method to study skeletal muscle with a new Fiji tool. Skelet Muscle [Internet]. 2018;8:25. Available from: http://www.ncbi.nlm.nih.gov/pubmed/30081940

62. Bendotti C, Baldessari S, Pende M, Southgate T, Guglielmetti F, Samanin R. Relationship between GAP-43 expression in the dentate gyrus and synaptic reorganization of hippocampal mossy fibres in rats treated with kainic acid. Eur J Neurosci [Internet]. 1997;9:93–101. Available from: http://www.ncbi.nlm.nih.gov/pubmed/9042573

63. Thacker JS, Yeung DH, Staines WR, Mielke JG. Total protein or high-abundance protein: Which offers the best loading control for Western blotting? Anal Biochem [Internet]. 2016;496:76–8. Available from: http://www.ncbi.nlm.nih.gov/pubmed/26706797

64. Ludolph AC, Bendotti C, Blaugrund E, Chio A, Greensmith L, Loeffler J-P, et al. Guidelines for preclinical animal research in ALS/MND: A consensus meeting. Amyotroph Lateral Scler [Internet]. 2010;11:38–45. Available from: http://www.ncbi.nlm.nih.gov/pubmed/20184514

65. Benkhelifa-Ziyyat S, Besse A, Roda M, Duque S, Astord S, Carcenac R, et al. Intramuscular scAAV9-SMN injection mediates widespread gene delivery to the spinal cord and decreases disease severity in SMA mice. Mol Ther [Internet]. The American Society of Gene & Cell Therapy; 2013;21:282–90. Available from: http://dx.doi.org/10.1038/mt.2012.261

66. Hegedus J, Putman CT, Gordon T. Time course of preferential motor unit loss in the SOD1G93A mouse model of amyotrophic lateral sclerosis. Neurobiol Dis [Internet]. 2007;28:154–64. Available from: https://linkinghub.elsevier.com/retrieve/pii/S0969996107001416

67. Clark JA, Southam KA, Blizzard CA, King AE, Dickson TC. Axonal degeneration, distal collateral branching and neuromuscular junction architecture alterations occur prior to symptom onset in the SOD1(G93A) mouse model of amyotrophic lateral sclerosis. J Chem Neuroanat [Internet]. 2016;76:35–47. Available from: https://linkinghub.elsevier.com/retrieve/pii/S0891061816300503

68. Loeffler JP, Picchiarelli G, Dupuis L, Gonzalez De Aguilar JL. The role of skeletal muscle in amyotrophic lateral sclerosis. Brain Pathol. 2016;26:227–36.

69. Campanari M-L, García-Ayllón M-S, Ciura S, Sáez-Valero J, Kabashi E. Neuromuscular Junction Impairment in Amyotrophic Lateral Sclerosis: Reassessing the Role of Acetylcholinesterase. Front Mol Neurosci [Internet]. 2016;9:160. Available from: http://www.ncbi.nlm.nih.gov/pubmed/28082868

70. Wier CG, Crum AE, Reynolds AB, Iyer CC, Chugh D, Palettas MS, et al. Muscle contractility dysfunction precedes loss of motor unit connectivity in SOD1(G93A) mice. Muscle Nerve [Internet]. 2019;59:254–62. Available from: http://www.ncbi.nlm.nih.gov/pubmed/30370671

71. Bruijn LII, Becher MWW, Lee MKK, Anderson KLL, Jenkins NAA, Copeland NGG, et al. ALS-Linked SOD1 Mutant G85R Mediates Damage to Astrocytes and Promotes Rapidly Progressive Disease with SOD1-Containing Inclusions. Neuron [Internet]. 1997;18:327–38. Available from: http://www.ncbi.nlm.nih.gov/pubmed/9052802

72. Dobrowolny G, Lepore E, Martini M, Barberi L, Nunn A, Scicchitano BM, et al. Metabolic Changes Associated With Muscle Expression of SOD1G93A. Front Physiol [Internet]. 2018;9:831. Available from: http://www.ncbi.nlm.nih.gov/pubmed/30042688

73. Dobrowolny G, Aucello M, Musarò A. Muscle atrophy induced by SOD1G93A expression does not involve the activation of caspase in the absence of denervation. Skelet Muscle [Internet]. 2011;1:3. Available from: http://www.ncbi.nlm.nih.gov/pubmed/21798081

74. Frey D, Schneider C, Xu L, Borg J, Spooren W, Caroni P. Early and selective loss of neuromuscular synapse subtypes with low sprouting competence in motoneuron diseases. J Neurosci [Internet]. 2000;20:2534–42. Available from: http://www.ncbi.nlm.nih.gov/pubmed/10729333

75. Harrison JM, Rafuse VF. Muscle fiber-type specific terminal Schwann cell pathology leads to sprouting deficits following partial denervation in SOD1G93A mice. Neurobiol Dis [Internet]. 2020;145:105052. Available from: http://www.ncbi.nlm.nih.gov/pubmed/32827689

76. Martineau É, Di Polo A, Vande Velde C, Robitaille R. Sex-Specific Differences in Motor-Unit Remodeling in a Mouse Model of ALS. eNeuro [Internet]. 2020;7. Available from: http://www.ncbi.nlm.nih.gov/pubmed/32033983

77. Gordon T, Hegedus J, Tam SL. Adaptive and maladaptive motor axonal sprouting in aging and motoneuron disease. Neurol Res [Internet]. 2004;26:174–85. Available from:

http://www.ncbi.nlm.nih.gov/pubmed/15072637

78. Lu H, Huang D, Saederup N, Charo IF, Ransohoff RM, Zhou L. Macrophages recruited via CCR2 produce insulin-like growth factor-1 to repair acute skeletal muscle injury. FASEB J [Internet]. 2011 [cited 2019 Sep 17];25:358–69. Available from: http://www.fasebj.org/doi/10.1096/fj.10-171579

79. Chazaud B. Inflammation and Skeletal Muscle Regeneration: Leave It to the Macrophages! Trends Immunol [Internet]. 2020; Available from: http://www.ncbi.nlm.nih.gov/pubmed/32362490

80. Wang HA, Lee JD, Lee KM, Woodruff TM, Noakes PG. Complement C5a-C5aR1 signalling drives skeletal muscle macrophage recruitment in the hSOD1G93A mouse model of amyotrophic lateral sclerosis. Skelet Muscle [Internet]. Skeletal Muscle; 2017;7:10. Available from: http://skeletalmusclejournal.biomedcentral.com/articles/10.1186/s13395-017-0128-8

81. Tonkin J, Temmerman L, Sampson RD, Gallego-Colon E, Barberi L, Bilbao D, et al. Monocyte/Macrophage-derived IGF-1 Orchestrates Murine Skeletal Muscle Regeneration and Modulates Autocrine Polarization. Mol Ther [Internet]. 2015;23:1189–200. Available from: http://www.ncbi.nlm.nih.gov/pubmed/25896247

82. Tonkin J, Villarroya F, Puri PL, Vinciguerra M. SIRT1 signaling as potential modulator of skeletal muscle diseases. Curr Opin Pharmacol [Internet]. 2012;12:372–6. Available from: http://www.ncbi.nlm.nih.gov/pubmed/22401932

83. Schug TT, Xu Q, Gao H, Peres-da-Silva A, Draper DW, Fessler MB, et al. Myeloid Deletion of SIRT1 Induces Inflammatory Signaling in Response to Environmental Stress. Mol Cell Biol [Internet]. 2010;30:4712–21. Available from: https://mcb.asm.org/content/30/19/4712

84. Luther SA, Cyster JG. Chemokines as regulators of T cell differentiation. Nat Immunol [Internet]. 2001;2:102–7. Available from: http://www.ncbi.nlm.nih.gov/pubmed/11175801

85. Tidball JG. Regulation of muscle growth and regeneration by the immune system. Nat Rev Immunol [Internet]. 2017;17:165–78. Available from: http://www.ncbi.nlm.nih.gov/pubmed/28163303

86. Oishi Y, Manabe I. Macrophages in inflammation, repair and regeneration. Int Immunol [Internet]. 2018;30:511–28. Available from: http://www.ncbi.nlm.nih.gov/pubmed/30165385

87. Castiglioni A, Corna G, Rigamonti E, Basso V, Vezzoli M, Monno A, et al. FOXP3+ T Cells Recruited to Sites of Sterile Skeletal Muscle Injury Regulate the Fate of Satellite Cells and Guide Effective Tissue Regeneration. PLoS One [Internet]. 2015;10:e0128094. Available from: http://www.ncbi.nlm.nih.gov/pubmed/26039259

88. Schiaffino S, Pereira MG, Ciciliot S, Rovere-Querini P. Regulatory T cells and skeletal muscle regeneration. FEBS J [Internet]. 2017;284:517–24. Available from: http://www.ncbi.nlm.nih.gov/pubmed/27479876

89. Teixeira CFP, Zamunér SR, Zuliani JP, Fernandes CM, Cruz-Hofling MA, Fernandes I, et al. Neutrophils do not contribute to local tissue damage, but play a key role in skeletal muscle regeneration, in mice injected with Bothrops asper snake venom. Muscle Nerve [Internet]. 2003;28:449–59. Available from: http://www.ncbi.nlm.nih.gov/pubmed/14506717

90. Tidball JG. Inflammatory cell response to acute muscle injury. Med Sci Sports Exerc [Internet]. 1995;27:1022–32. Available from: http://www.ncbi.nlm.nih.gov/pubmed/7564969

91. Arnold L, Henry A, Poron F, Baba-Amer Y, van Rooijen N, Plonquet A, et al. Inflammatory monocytes recruited after skeletal muscle injury switch into antiinflammatory macrophages to support myogenesis. J Exp Med [Internet]. 2007;204:1057–69. Available from: http://www.ncbi.nlm.nih.gov/pubmed/17485518

92. Kharraz Y, Guerra J, Mann CJ, Serrano AL, Muñoz-Cánoves P. Macrophage plasticity and the role of inflammation in skeletal muscle repair. Mediators Inflamm [Internet]. 2013;2013:491497. Available from: http://www.ncbi.nlm.nih.gov/pubmed/23509419

93. Saclier M, Yacoub-Youssef H, Mackey AL, Arnold L, Ardjoune H, Magnan M, et al. Differentially activated macrophages orchestrate myogenic precursor cell fate during human skeletal muscle regeneration. Stem Cells. 2013;31:384–96.

94. Patsalos A, Pap A, Varga T, Trencsenyi G, Contreras GA, Garai I, et al. In situ macrophage phenotypic transition is affected by altered cellular composition prior to acute sterile muscle injury. J Physiol [Internet]. 2017;595:5815–42. Available from: http://www.ncbi.nlm.nih.gov/pubmed/28714082

95. Mauro A. SATELLITE CELL OF SKELETAL MUSCLE FIBERS. J Biophys Biochem Cytol [Internet]. 1961;9:493–5. Available from: https://rupress.org/jcb/article/9/2/493/19539/SATELLITE-CELL-OF-SKELETAL-MUSCLE-FIBERS

96. Cornelison DD, Wold BJ. Single-cell analysis of regulatory gene expression in quiescent and activated mouse skeletal muscle satellite cells. Dev Biol [Internet]. 1997;191:270–83. Available from: http://www.ncbi.nlm.nih.gov/pubmed/9398440

97. Relaix F, Zammit PS. Satellite cells are essential for skeletal muscle regeneration: the cell on the edge returns centre stage. Development [Internet]. 2012;139:2845–56. Available from: http://dev.biologists.org/cgi/doi/10.1242/dev.069088

98. Forcina L, Miano C, Pelosi L, Musarò A. An Overview About the Biology of Skeletal Muscle Satellite Cells. Curr Genomics [Internet]. 2019;20:24–37. Available from: http://www.eurekaselect.com/169026/article

99. Folker ES, Baylies MK. Nuclear positioning in muscle development and disease. Front Physiol [Internet]. 2013;4:363. Available from: http://www.ncbi.nlm.nih.gov/pubmed/24376424

100. Hegedus J, Putman CT, Tyreman N, Gordon T. Preferential motor unit loss in the SOD1 G93A transgenic mouse model of amyotrophic lateral sclerosis. J Physiol [Internet]. 2008;586:3337–51. Available from: http://www.ncbi.nlm.nih.gov/pubmed/18467368

101. Palamiuc L, Schlagowski A, Ngo ST, Vernay A, Dirrig-Grosch S, Henriques A, et al. A metabolic switch toward lipid use in glycolytic muscle is an early pathologic event in a mouse model of amyotrophic lateral sclerosis. EMBO Mol Med [Internet]. 2015;7:526–46. Available from: http://www.ncbi.nlm.nih.gov/pubmed/25820275

102. Song X-Y, Zhou FH-H, Zhong J-H, Wu LLY, Zhou X-F. Knockout of p75(NTR) impairs re-myelination of injured sciatic nerve in mice. J Neurochem [Internet]. 2006;96:833–42. Available from: http://www.ncbi.nlm.nih.gov/pubmed/16336221

103. Butovsky O, Siddiqui S, Gabriely G, Lanser AJ, Dake B, Murugaiyan G, et al. Modulating inflammatory monocytes with a unique microRNA gene signature ameliorates murine ALS. J Clin Invest [Internet]. 2012;122:3063–87. Available from: http://www.ncbi.nlm.nih.gov/pubmed/22863620

104. Sargsyan SA, Blackburn DJ, Barber SC, Monk PN, Shaw PJ. Mutant SOD1 G93A microglia have an inflammatory phenotype and elevated production of MCP-1. Neuroreport [Internet]. 2009;20:1450–5. Available from: http://www.ncbi.nlm.nih.gov/pubmed/19752764

105. Henkel JS, Beers DR, Zhao W, Appel SH. Microglia in ALS: The Good, The Bad, and The Resting. J Neuroimmune Pharmacol [Internet]. 2009;4:389–98. Available from: http://link.springer.com/10.1007/s11481-009-9171-5

106. Beers DR, Henkel JS, Zhao W, Wang J, Huang A, Wen S, et al. Endogenous regulatory T lymphocytes ameliorate amyotrophic lateral sclerosis in mice and correlate with disease progression in patients with amyotrophic lateral sclerosis. Brain [Internet]. 2011;134:1293–314. Available from: http://www.ncbi.nlm.nih.gov/pubmed/21596768

107. Gurney ME. The use of transgenic mouse models of amyotrophic lateral sclerosis in preclinical drug studies. J Neurol Sci [Internet]. 1997;152:s67–73. Available from: https://linkinghub.elsevier.com/retrieve/pii/S0022510X97002475

108. Gurney ME, Pu H, Chiu AY, Dal Canto MC, Polchow CY, Alexander DD, et al. Motor neuron degeneration in mice that express a human Cu,Zn superoxide dismutase mutation. Science [Internet]. 1994;264:1772–5. Available from: http://www.ncbi.nlm.nih.gov/pubmed/8209258

109. Bendotti C, Carrì MT. Lessons from models of SOD1-linked familial ALS [Internet]. Trends Mol. Med. 2004. p. 393–400. Available from: https://linkinghub.elsevier.com/retrieve/pii/S1471491404001595

110. Schäfer S, Hermans E. Reassessment of motor-behavioural test analyses enables the detection of early disease-onset in a transgenic mouse model of amyotrophic lateral sclerosis. Behav Brain Res

[Internet]. 2011;225:7–14. Available from: https://linkinghub.elsevier.com/retrieve/pii/S0166432811004827

111. Deshmane SL, Kremlev S, Amini S, Sawaya BE. Monocyte Chemoattractant Protein-1 (MCP-1): An Overview. J Interf Cytokine Res [Internet]. 2009;29:313–26. Available from: http://www.liebertpub.com/doi/10.1089/jir.2008.0027

112. Conductier G, Blondeau N, Guyon A, Nahon J-L, Rovère C. The role of monocyte chemoattractant protein MCP1/CCL2 in neuroinflammatory diseases. J Neuroimmunol [Internet]. 2010;224:93–100. Available from: http://www.ncbi.nlm.nih.gov/pubmed/20681057

113. Sawyer AJ, Tian W, Saucier-Sawyer JK, Rizk PJ, Saltzman WM, Bellamkonda R V, et al. The effect of inflammatory cell-derived MCP-1 loss on neuronal survival during chronic neuroinflammation. Biomaterials [Internet]. 2014;35:6698–706. Available from: http://www.ncbi.nlm.nih.gov/pubmed/24881026

114. Semple BD, Frugier T, Morganti-Kossmann MC. CCL2 modulates cytokine production in cultured mouse astrocytes. J Neuroinflammation [Internet]. 2010;7:67. Available from: http://www.ncbi.nlm.nih.gov/pubmed/20942978

115. Wilms H, Sievers J, Dengler R, Bufler J, Deuschl G, Lucius R. Intrathecal synthesis of monocyte chemoattractant protein-1 (MCP-1) in amyotrophic lateral sclerosis: further evidence for microglial activation in neurodegeneration. J Neuroimmunol [Internet]. 2003;144:139–42. Available from: https://linkinghub.elsevier.com/retrieve/pii/S0165572803003576

116. Baron P, Bussini S, Cardin V, Corbo M, Conti G, Galimberti D, et al. Production of monocyte chemoattractant protein-1 in amyotrophic lateral sclerosis. Muscle Nerve [Internet]. 2005;32:541–4. Available from: http://www.ncbi.nlm.nih.gov/pubmed/15962273

117. Nagata T, Nagano I, Shiote M, Narai H, Murakami T, Hayashi T, et al. Elevation of MCP-1 and MCP-1/VEGF ratio in cerebrospinal fluid of amyotrophic lateral sclerosis patients. Neurol Res [Internet]. 2007;29:772–6. Available from: http://www.tandfonline.com/doi/full/10.1179/016164107X229795

118. Tofaris GK, Patterson PH, Jessen KR, Mirsky R. Denervated Schwann cells attract macrophages by secretion of leukemia inhibitory factor (LIF) and monocyte chemoattractant protein-1 in a process regulated by interleukin-6 and LIF. J Neurosci [Internet]. 2002;22:6696–703. Available from: http://www.ncbi.nlm.nih.gov/pubmed/12151548

119. Kwon MJ, Shin HY, Cui Y, Kim H, Le Thi AH, Choi JY, et al. CCL2 mediates neuron-macrophage interactions to drive proregenerative macrophage activation following preconditioning injury. J Neurosci. 2015;35:15934–47.

120. Stratton JA, Eaton S, Rosin NL, Jawad S, Holmes A, Yoon G, et al. Macrophages and Associated Ligands in the Aged Injured Nerve: A Defective Dynamic That Contributes to Reduced Axonal Regrowth. Front Aging Neurosci [Internet]. 2020;12. Available from: https://www.frontiersin.org/article/10.3389/fnagi.2020.00174/full

121. Shiraishi W, Yamasaki R, Hashimoto Y, Ko S, Kobayakawa Y, Isobe N, et al. Clearance of peripheral nerve misfolded mutant protein by infiltrated macrophages correlates with motor neuron disease progression. Sci Rep [Internet]. 2021;11:16438. Available from: http://www.ncbi.nlm.nih.gov/pubmed/34385589

122. Lu H, Huang D, Ransohoff RM, Zhou L. Acute skeletal muscle injury: CCL2 expression by both monocytes and injured muscle is required for repair. FASEB J [Internet]. 2011;25:3344–55. Available from: http://www.ncbi.nlm.nih.gov/pubmed/21697550

123. Lincecum JM, Vieira FG, Wang MZ, Thompson K, De Zutter GS, Kidd J, et al. From transcriptome analysis to therapeutic anti-CD40L treatment in the SOD1 model of amyotrophic lateral sclerosis. Nat Genet [Internet]. 2010;42:392–9. Available from: http://www.ncbi.nlm.nih.gov/pubmed/20348957

124. Graber DJ, Hickey WF, Harris BT. Progressive changes in microglia and macrophages in spinal cord and peripheral nerve in the transgenic rat model of amyotrophic lateral sclerosis. J Neuroinflammation [Internet]. 2010;7:8. Available from: http://www.ncbi.nlm.nih.gov/pubmed/20109233

125. Vasco C, Canazza A, Rizzo A, Mossa A, Corsini E, Silvani A, et al. Circulating T regulatory cells migration and phenotype in glioblastoma patients: an in vitro study. J Neurooncol [Internet]. 2013;115:353–63. Available from: http://www.ncbi.nlm.nih.gov/pubmed/24005771

126. Burzyn D, Kuswanto W, Kolodin D, Shadrach JL, Cerletti M, Jang Y, et al. A special population of regulatory T cells potentiates muscle repair. Cell [Internet]. 2013;155:1282–95. Available from: http://www.ncbi.nlm.nih.gov/pubmed/24315098

127. Villalta SA, Rosenthal W, Martinez L, Kaur A, Sparwasser T, Tidball JG, et al. Regulatory T cells suppress muscle inflammation and injury in muscular dystrophy. Sci Transl Med [Internet]. 2014;6:258ra142-258ra142. Available from: https://stm.sciencemag.org/lookup/doi/10.1126/scitranslmed.3009925

128. Arecco N, Clarke CJ, Jones FK, Simpson DM, Mason D, Beynon RJ, et al. Elastase levels and activity are increased in dystrophic muscle and impair myoblast cell survival, proliferation and differentiation. Sci Rep [Internet]. 2016;6:24708. Available from: http://www.nature.com/articles/srep24708

129. Tidball JG, Dorshkind K, Wehling-Henricks M. Shared signaling systems in myeloid cell-mediated muscle regeneration. Dev [Internet]. 2014;141:1184–96. Available from: http://www.ncbi.nlm.nih.gov/pubmed/24595286

130. Howard EE, Pasiakos SM, Blesso CN, Fussell MA, Rodriguez NR. Divergent Roles of Inflammation in Skeletal Muscle Recovery From Injury. Front Physiol [Internet]. 2020;11:87. Available from: http://www.ncbi.nlm.nih.gov/pubmed/32116792

131. White P, Liebhaber SA, Cooke NE. 129X1/SvJ Mouse Strain Has a Novel Defect in Inflammatory Cell Recruitment. J Immunol [Internet]. 2002;168:869–74. Available from: http://www.jimmunol.org/lookup/doi/10.4049/jimmunol.168.2.869

132. Hoover-Plow JL, Gong Y, Shchurin A, Busuttil SJ, Schneeman TA, Hart E. Strain and model dependent differences in inflammatory cell recruitment in mice. Inflamm Res [Internet]. 2008;57:457–63. Available from: http://www.ncbi.nlm.nih.gov/pubmed/18827970

133. Rizzo G, Di Maggio R, Benedetti A, Morroni J, Bouche M, Lozanoska-Ochser B. Splenic Ly6Chi monocytes are critical players in dystrophic muscle injury and repair. JCI insight [Internet]. 2020;5. Available from: https://insight.jci.org/articles/view/130807

134. Niemi JP, DeFrancesco-Lisowitz A, Cregg JM, Howarth M, Zigmond RE. Overexpression of the monocyte chemokine CCL2 in dorsal root ganglion neurons causes a conditioning-like increase in neurite outgrowth and does so via a STAT3 dependent mechanism. Exp Neurol [Internet]. 2016;275 Pt 1:25–37. Available from: http://www.ncbi.nlm.nih.gov/pubmed/26431741

135. Kunis G, Baruch K, Miller O, Schwartz M. Immunization with a Myelin-Derived Antigen Activates the Brain's Choroid Plexus for Recruitment of Immunoregulatory Cells to the CNS and Attenuates Disease Progression in a Mouse Model of ALS. J Neurosci [Internet]. 2015;35:6381–93. Available from: http://www.jneurosci.org/cgi/doi/10.1523/JNEUROSCI.3644-14.2015

136. Chiot A, Zaïdi S, Iltis C, Ribon M, Berriat F, Schiaffino L, et al. Modifying macrophages at the periphery has the capacity to change microglial reactivity and to extend ALS survival. Nat Neurosci [Internet]. 2020; Available from: http://www.ncbi.nlm.nih.gov/pubmed/33077946

137. Gois AM, Mendonça DMF, Freire MAM, Santos JR. IN VITRO AND IN VIVO MODELS OF AMYOTROPHIC LATERAL SCLEROSIS: AN UPDATED OVERVIEW. Brain Res Bull [Internet]. 2020;159:32–43. Available from: http://www.ncbi.nlm.nih.gov/pubmed/32247802

138. Liguori F, Amadio S, Volonté C. Where and Why Modeling Amyotrophic Lateral Sclerosis. Int J Mol Sci [Internet]. 2021;22. Available from: http://www.ncbi.nlm.nih.gov/pubmed/33921446

139. Liu Z, Cheng X, Zhong S, Zhang X, Liu C, Liu F, et al. Peripheral and Central Nervous System Immune Response Crosstalk in Amyotrophic Lateral Sclerosis. Front Neurosci [Internet]. 2020;14:575. Available from: http://www.ncbi.nlm.nih.gov/pubmed/32612503

140. Béland L-C, Markovinovic A, Jakovac H, De Marchi F, Bilic E, Mazzini L, et al. Immunity in amyotrophic lateral sclerosis: blurred lines between excessive inflammation and inefficient immune

responses. Brain Commun [Internet]. 2020;2. Available from: https://academic.oup.com/braincomms/article/doi/10.1093/braincomms/fcaa124/5892251

141. McCombe PA, Henderson RD. The Role of immune and inflammatory mechanisms in ALS. Curr Mol Med [Internet]. 2011;11:246–54. Available from: http://www.eurekaselect.com/openurl/content.php?genre=article&issn=1566-5240&volume=11&issue=3&spage=246

142. Riva N, Clarelli F, Domi T, Cerri F, Gallia F, Trimarco A, et al. Unraveling gene expression profiles in peripheral motor nerve from amyotrophic lateral sclerosis patients: Insights into pathogenesis. Sci Rep. 2016;6:1–15.

Figures

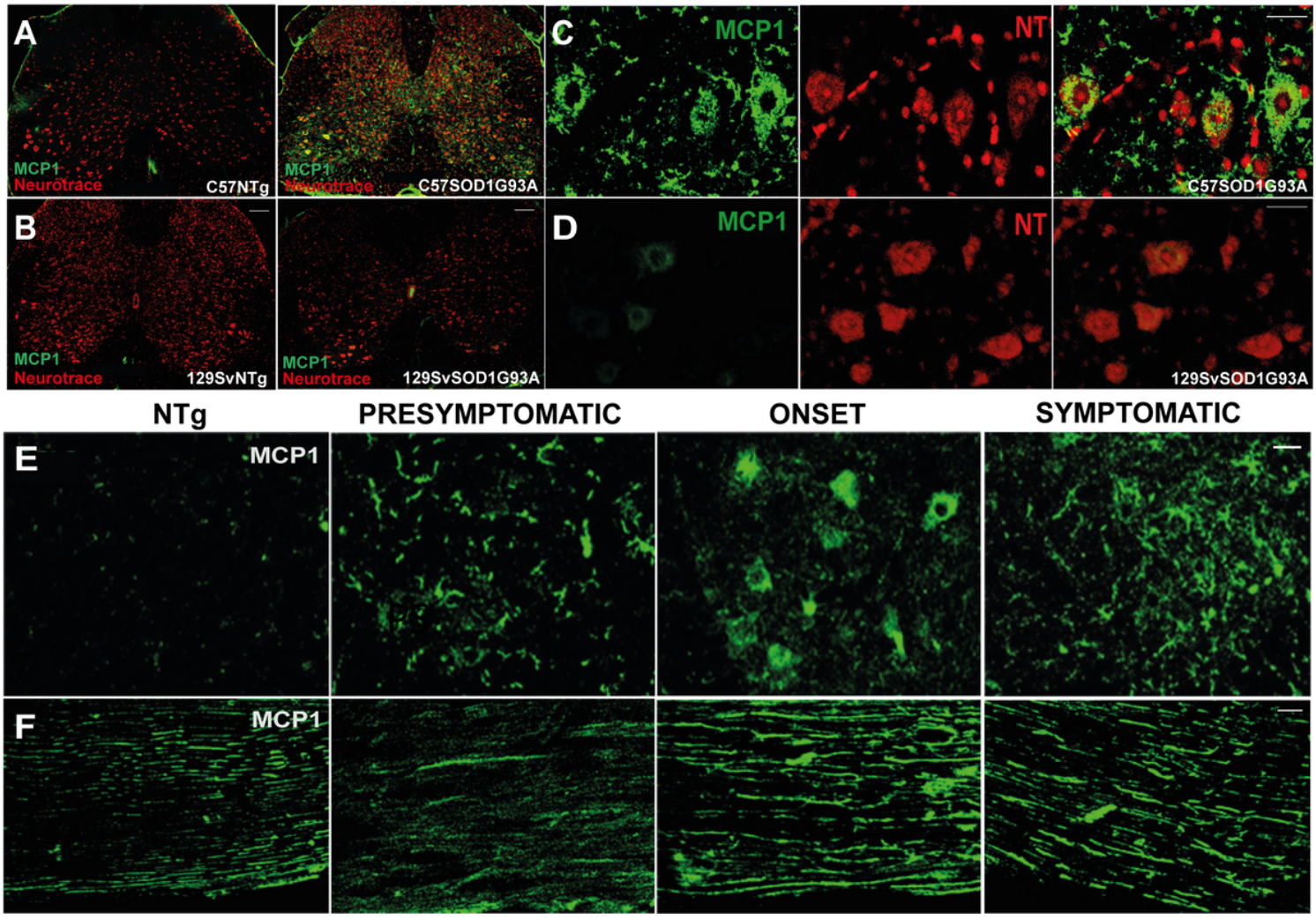

Figure 1

MCP1 expression pattern in the CNS and PNS of fast- and slow-progressing SOD1G93A mice. A-D MCP1 expression (green) is strictly upregulated in the lumbar spinal cord of C57SOD1G93A compared with 129SvSOD1G93A mice at the disease onset (NT, neurotrace; red). Scale bar, (A, B) 100μm; (C, D) 50μm. E,

F MCP1 expression gradually increases in the lumbar spinal cord (E) and sciatic nerve (F) of C57SOD1G93A mice as the disease progresses. Scale bar, 100μm. The qualitative histological analysis was performed on 4/6 serial sections of the L3-L5 spinal cord or sciatic nerve from at least n=3 mice per strain and genotype at each time point.

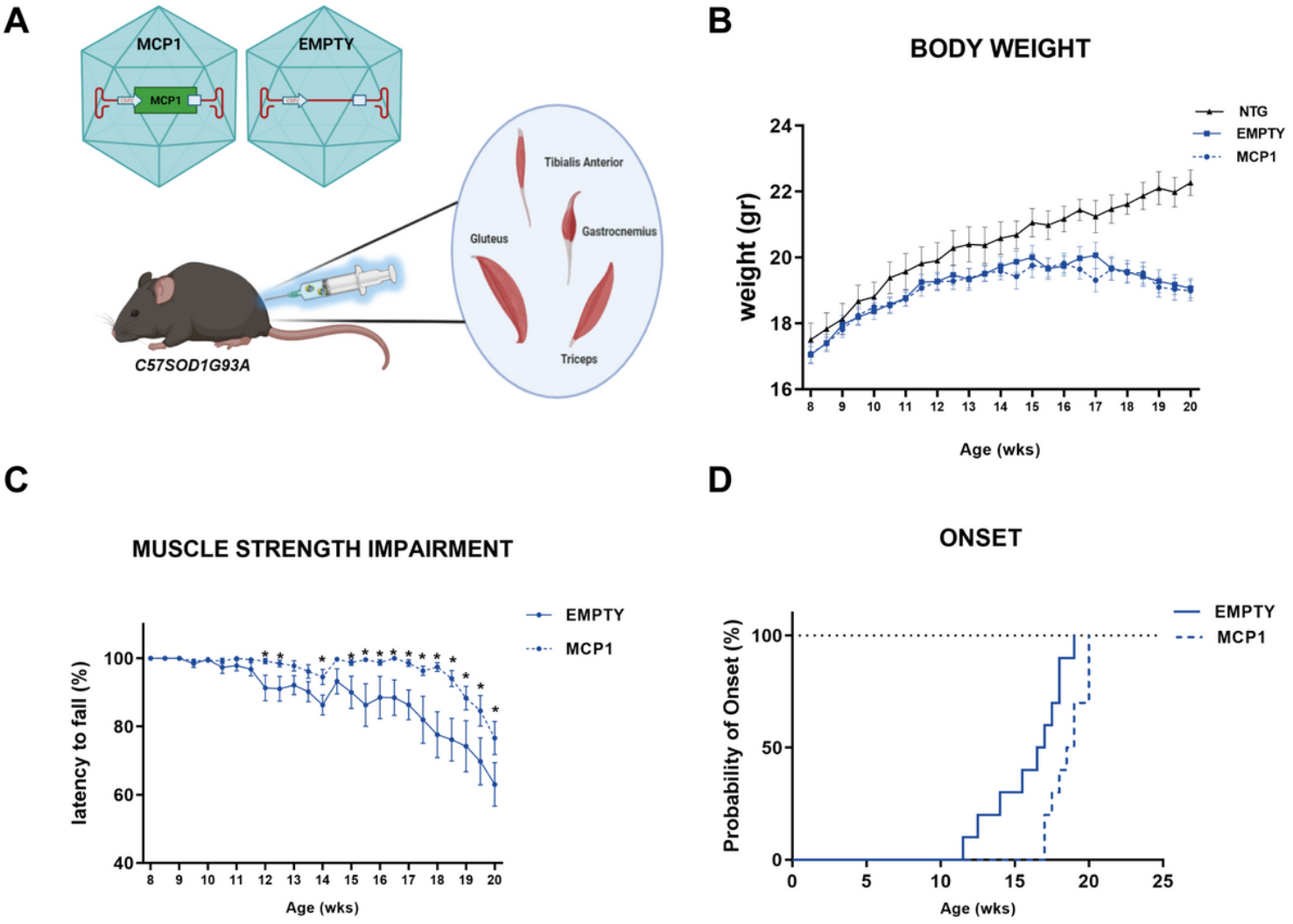

Figure 2

The scAAV9_MCP1 injection ameliorates the disease progression of C57SOD1G93A mice. A Experimental design. The engineered (scAAV9_MCP1) or empty (scAAV9(empty)) vector was administered in both hindlimb and forelimb muscles of 8 weeks-old C57SOD1G93A mice (n=18 per experimental group). Image Created in Biorender.com. B, C Recording of (B) body weight and (C) muscle strength impairment of scAAV9_MCP1- and scAAV9(empty)-treated mice until the symptomatic disease stage. Data are reported as mean±SEM for each time point. *p < 0.05; by repeated-measures ANOVA with Sidak's post-analysis. D scAAV9_MCP1-treated mice exhibit a postponement of the disease onset of ~2 weeks compared with the scAAV9(empty) group. Age of disease onset: Empty 16±0.8 weeks, MCP1 18.6±0.4 weeks. mean±SEM. p=0.0088 by Mantel-Cox log-rank test.

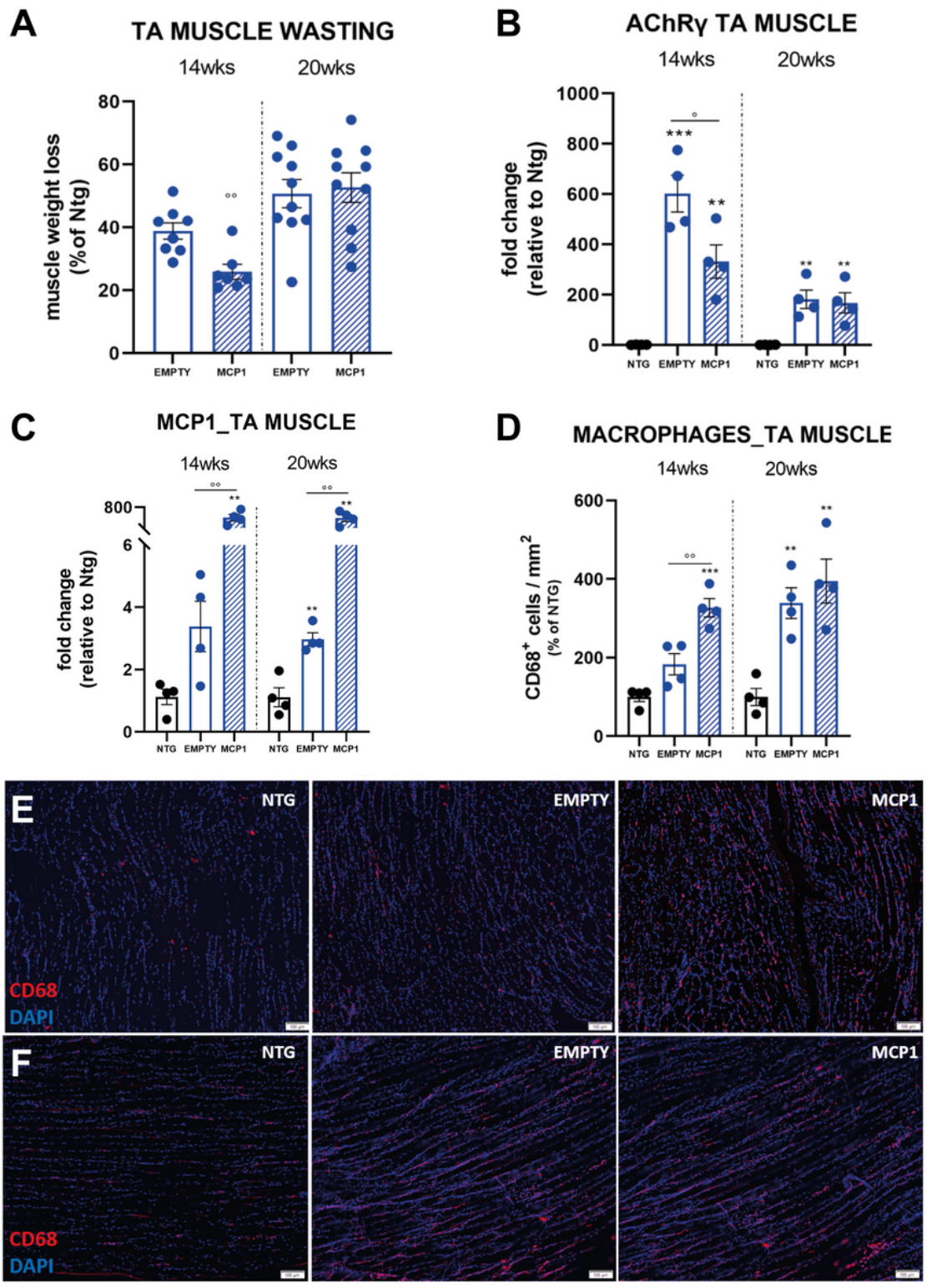

Figure 3

The scAAV9_MCP1 injection in C57SOD1G93A mice delays the hindlimb muscles degeneration, promoting macrophage recruitment. A Muscle wasting was calculated by measuring the TA muscle weight of scAAV9_MCP1- and scAAV9(empty)-treated mice compared to relative Ntg littermates at each time points analysed. The percentage of muscle atrophy was calculated relative to Ntg mice. Data are reported as mean±SEM. n=8 per experimental group at 14 weeks; n=10 per experimental group at 20

weeks. B, C Real-time PCR analysis of AChRγ (B) and Mcp1 transcript (C) in the TA muscle of scAAV9_MCP1- and scAAV9(empty)-treated mice compared to relative Ntg littermates. Data are normalised to β-actin and expressed as mean±SEM. n=4 per experimental group at each time point. D-F Representative confocal micrographs of longitudinal sections of TA muscle of scAAV9_MCP1- and scAAV9(empty)-treated mice and Ntg littermates at (E) 14 and (F) 20 weeks stained with the phagocytic marker CD68 (red) and DAPI (nucleus, blue). Scale bar, 100μm. (D) The relative quantifications demonstrate an increased macrophage infiltration in the TA muscle of scAAV9_MCP1-treated mice compared with the scAAV9(empty) group at 14 but not 20 weeks. Data are reported as mean±SEM of 3/5 serials sections per muscle from n=4 mice per experimental group at each time point. *p<0.05, **p<0.01, ***p<0.001 Ntg Vs EMPTY or MCP1; °p<0.05, °°p<0.01 EMPTY Vs MCP1 by one-way ANOVA with Fisher post-analysis.

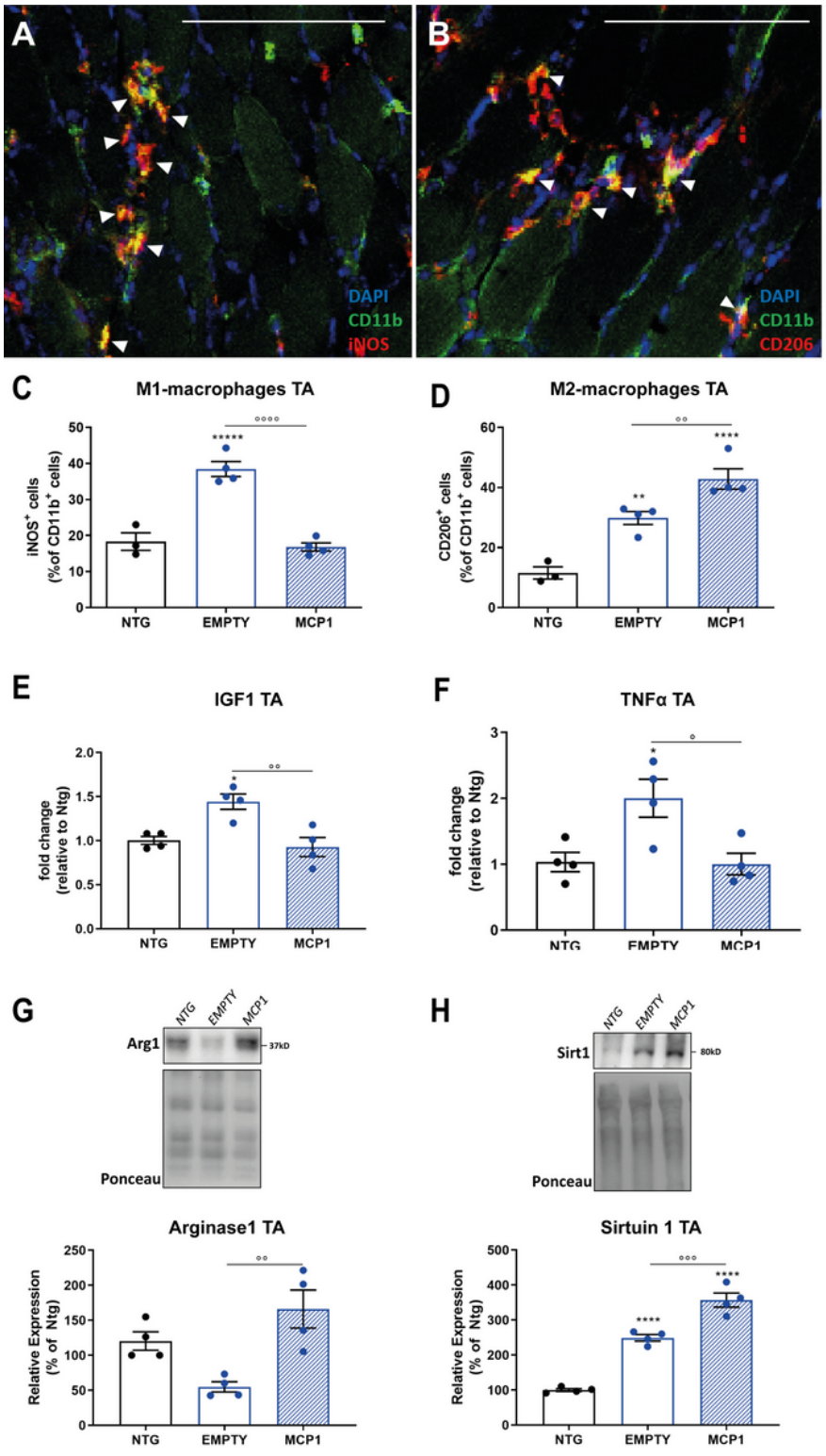

Figure 4

The MCP1 boosting enables the macrophage phenotypic switch in the hindlimb muscles of C57SOD1G93A mice. A-D Representative confocal micrographs of coronal sections of TA muscle of scAAV9_MCP1- and scAAV9(empty)-treated mice and Ntg littermates at 14 weeks stained with the myeloid marker CD11b (green), (A) the pro-inflammatory iNOS (red) or (B) anti-inflammatory CD206 (red) marker and DAPI (nucleus, blue). White arrowheads indicate CD11b+CD206+ or CD11b+iNOS+

macrophages. Scale bar, 100μm. The relative quantifications show a decreasing percentage of (C) M1 pro-inflammatory and a compensatory increase of (D) M2 anti-inflammatory macrophages in scAAV9_MCP1- compared with scAAV9(empty)-treated mice. Data are reported as mean±SEM of 3/5 serials sections per muscle from n=3 Ntg and n=4 SOD1G93A mice per group. E, F The Real-time PCR analysis shows a downregulated transcription of (E) Igf1 and (F) Tnfα in the TA muscle of scAAV9_MCP1- compared with scAAV9(empty)-treated mice at 14 weeks. Data are normalised to β-actin and expressed as fold change relative to the Ntg mice. n=4 per group. G, H Representative immunoblot images and relative quantifications of (G) Arginase 1 and (H) Sirtuin 1 expression in the TA muscle of scAAV9_MCP1- and scAAV9(empty)-treated mice and Ntg littermates at 14 weeks. Both proteins resulted significantly upregulated in the hind paw muscle of scAAV9_MCP1-treated mice compared with the control groups. n=4 per experimental group. Data are reported as mean±SEM. *p<0.05, **p<0.01, ****p<0.0001 Ntg Vs EMPTY or MCP1; °p<0.05, °°p<0.01, °°°p<0.001, °°°°p<0.0001 EMPTY Vs MCP1 by one-way ANOVA with Fisher post-analysis.

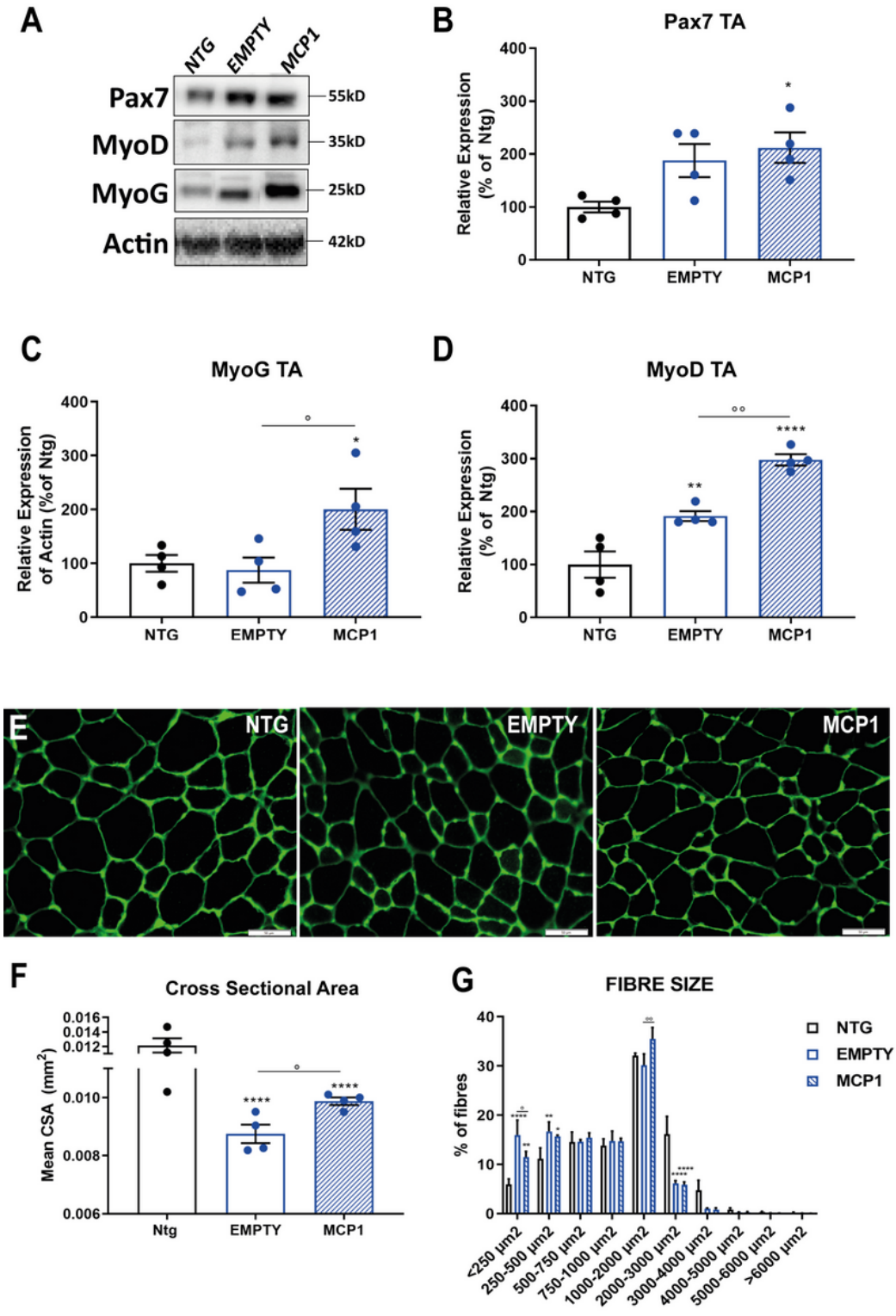

Figure 5

The MCP1-mediated immune response triggers the myogenic programme in the hindlimb muscles of C57SOD1G93A mice. A Representative immunoblot images of Pax7, MyoG and MyoD expression in TA muscle extracts of scAAV9_MCP1- and scAAV9(empty)-treated mice and Ntg littermates at 14 weeks. B-D The densitometric analysis shows an increased expression of (C) MyoG and (D) MyoD, but not (B) Pax7, in the hid paw muscle of scAAV9_MCP1-treated mice compared with the scAAV9(empty) group. n=4 per

experimental group. E Representative confocal micrograph of coronal sections of the TA muscle of scAAV9_MCP1- and scAAV9(empty)-treated mice and Ntg littermates at 14 weeks stained with Laminin (green). Scale bar, 50µm. F, G Quantitative analysis of (F) the TA muscle fibres cross-sectional area (CSA) mean and (G) size distribution shows preservation of the hind paw muscle of scAAV9_MCP1-treated mice compared with scAAV9(empty) group. Data are reported as mean±SEM of 3/5 serials sections per muscle from n=4 mice per group. *p<0.05, **p<0.01, ****p<0.0001 Ntg Vs EMPTY or MCP1; °p<0.05, °°p<0.01, EMPTY Vs MCP1 by (B, C, D, F) one-way or (G) two-way ANOVA with Fisher post-analysis.

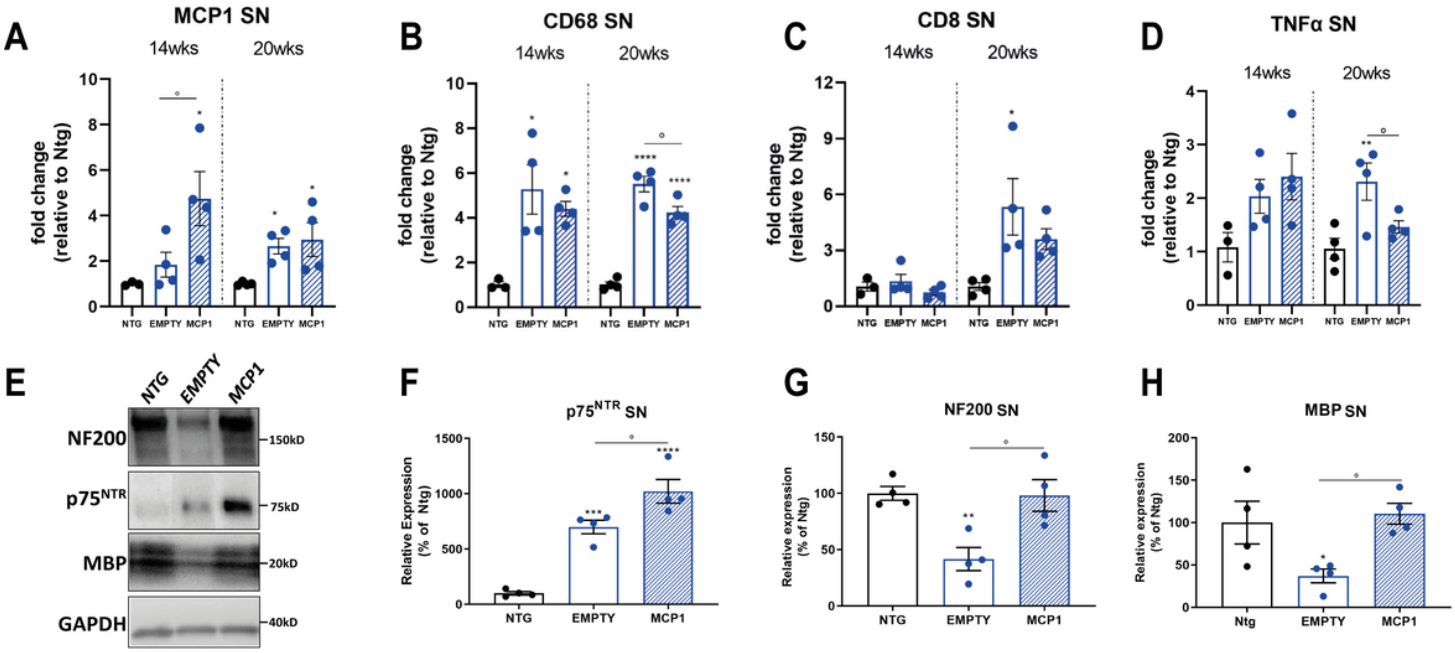

Figure 6

The MCP1 boosting preserved motor axon from demyelination in the sciatic nerve of C57SOD1G93A mice. A-D Real-time PCR analysis of (A) Mcp1, (B) CD68, (C) CD8a and (D) CD4 transcript in the sciatic nerve (SN) of scAAV9_MCP1- and scAAV9(empty)-treated mice compared to relative Ntg littermates. Data are normalised to β-actin and expressed as mean±SEM. 14 weeks: n=3 Ntg and n=4 SOD1G93A mice per group; 20 weeks: n=4 per experimental group. E Representative immunoblot images of NF200, p75NTR and MBP expression in SN extracts of scAAV9_MCP1- and scAAV9(empty)-treated mice and Ntg littermates at 20 weeks. F-H The densitometric analysis shows an increased expression of (F) p75NTR, (G) NF200 and (H) MBP in the SN of scAAV9_MCP1-treated mice compared with the scAAV9(empty) group. Data are reported as mean±SEM. n=4 per experimental group. *p<0.05, **p<0.01, ***p<0.001, ****p<0.0001 Ntg Vs EMPTY or MCP1; °p<0.05, EMPTY Vs MCP1 by one-way ANOVA with Fisher post-analysis.

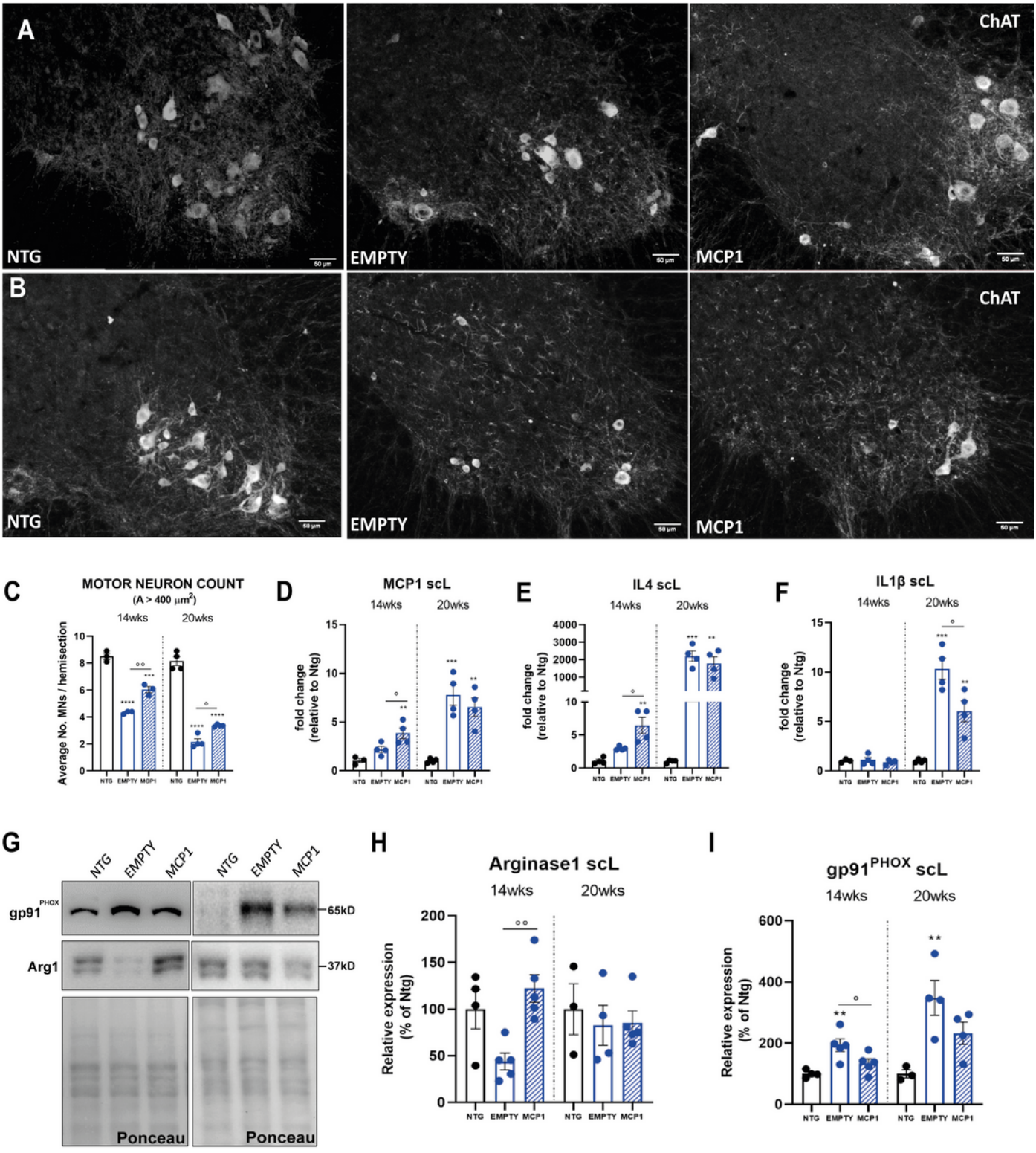

Figure 7

The MCP1 induction prevents motoneuron degeneration and modulates neuroinflammation in the CNS of C57SOD1G93A mice. A, B Representative ChAT-stained coronal sections of the lumbar spinal cord of scAAV9_MCP1- and scAAV9(empty)-treated mice and Ntg littermates at (A) 14 weeks and (B) 20 weeks. Scale bar, 50μm. C Motor neuron counts. Data are expressed as mean±SEM of MNs (Area ≥ 400 μm2) counted per section. The quantitative analysis was performed on 12 serial ChAT-stained sections of the

L3-L5 spinal cord segment. 14 weeks: n=3 per group; 20 weeks: n=4 per group. D-F Real-time PCR analysis of (D) Mcp1, (E) Il4, and (F) Il1β transcript in the lumbar spinal cord of scAAV9_MCP1- and scAAV9(empty)-treated mice compared to relative Ntg littermates at 14 and 20 weeks. Data are normalised to β-actin and expressed as mean±SEM. n=4 per experimental group. G-I Representative immunoblot images and relative densitometric analysis of (G, H) Arginase1 and (G, I) gp91PHOX expression in lumbar spinal cord extracts of scAAV9_MCP1- and scAAV9(empty)-treated mice and Ntg littermates at 14 and 20 weeks. Data are reported as mean±SEM. 14 weeks: n=4 per experimental group; 20 weeks: n=3 Ntg and n=4 SOD1G93A mice per group. **p<0.01, ***p<0.001, ****p<0.0001 Ntg Vs EMPTY or MCP1; °p<0.05, °°p<0.01 EMPTY Vs MCP1 by one-way ANOVA with Fisher post-analysis.

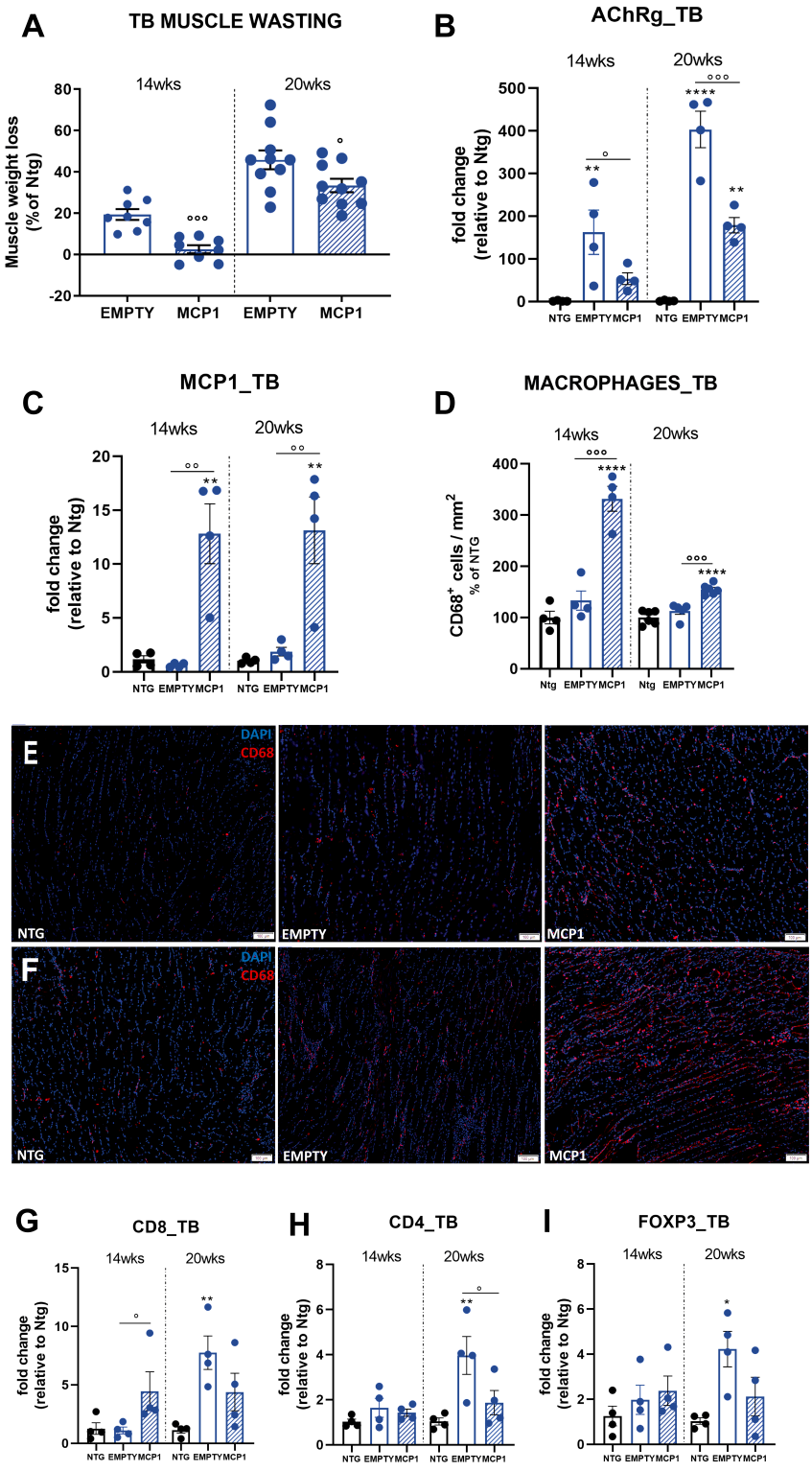

Figure 8

The scAAV9_MCP1 injection reduces the forelimb muscles degeneration promoting leucocytes recruitment in C57SOD1G93A mice. A Muscle wasting was calculated by measuring the TB muscle weight of scAAV9_MCP1- and scAAV9(empty)-treated mice compared to relative Ntg littermates at each time points analysed. The percentage of muscle atrophy was calculated relative to Ntg mice. Data are reported as mean±SEM. 14 weeks: n=8 per group; 20 weeks: n=10 per group. B, C The real-time PCR

analysis shows (B) significant downregulation of AChRγ and (C) dramatic increase of Mcp1 transcript in the TB muscle of scAAV9_MCP1-treated mice compared with the scAAV9(empty) group at both 14 and 20 weeks. Data are normalised to β-actin and expressed as mean±SEM. n=4 per experimental group at each time point analysed. D-F Quantification and representative confocal micrograph of longitudinal sections of TB muscle of scAAV9_MCP1- and scAAV9(empty)-treated mice and Ntg littermates at (D, E) 14 and (D, F) 20 weeks stained with the phagocytic marker CD68 (red) and DAPI (nucleus, blue). Scale bar, 100μm. The histological analysis shows a significant increase of macrophages infiltration in the forepaw muscle of scAAV9_MCP1-treated mice compared with the scAAV9(empty) group at both time points. Data are reported as mean±SEM of 3/5 serial sections per muscle from n=4 mice per group at 14 weeks and n=6 mice per group at 20 weeks. G-I Real-time PCR analysis of (G) CD8a, (H) CD4 and (I) Foxp3 transcript in the TB muscle of scAAV9_MCP1- and scAAV9(empty)-treated mice compared to relative Ntg littermates at 14 and 20 weeks. Data are normalised to β-actin and expressed as mean±SEM. n=4 per experimental group at each time point. *p<0.05, **p<0.01, ****p<0.0001 Ntg Vs EMPTY or MCP1; °p<0.05, °°p<0.01, °°°p<0.001 EMPTY Vs MCP1 by one-way ANOVA with Fisher post-analysis.

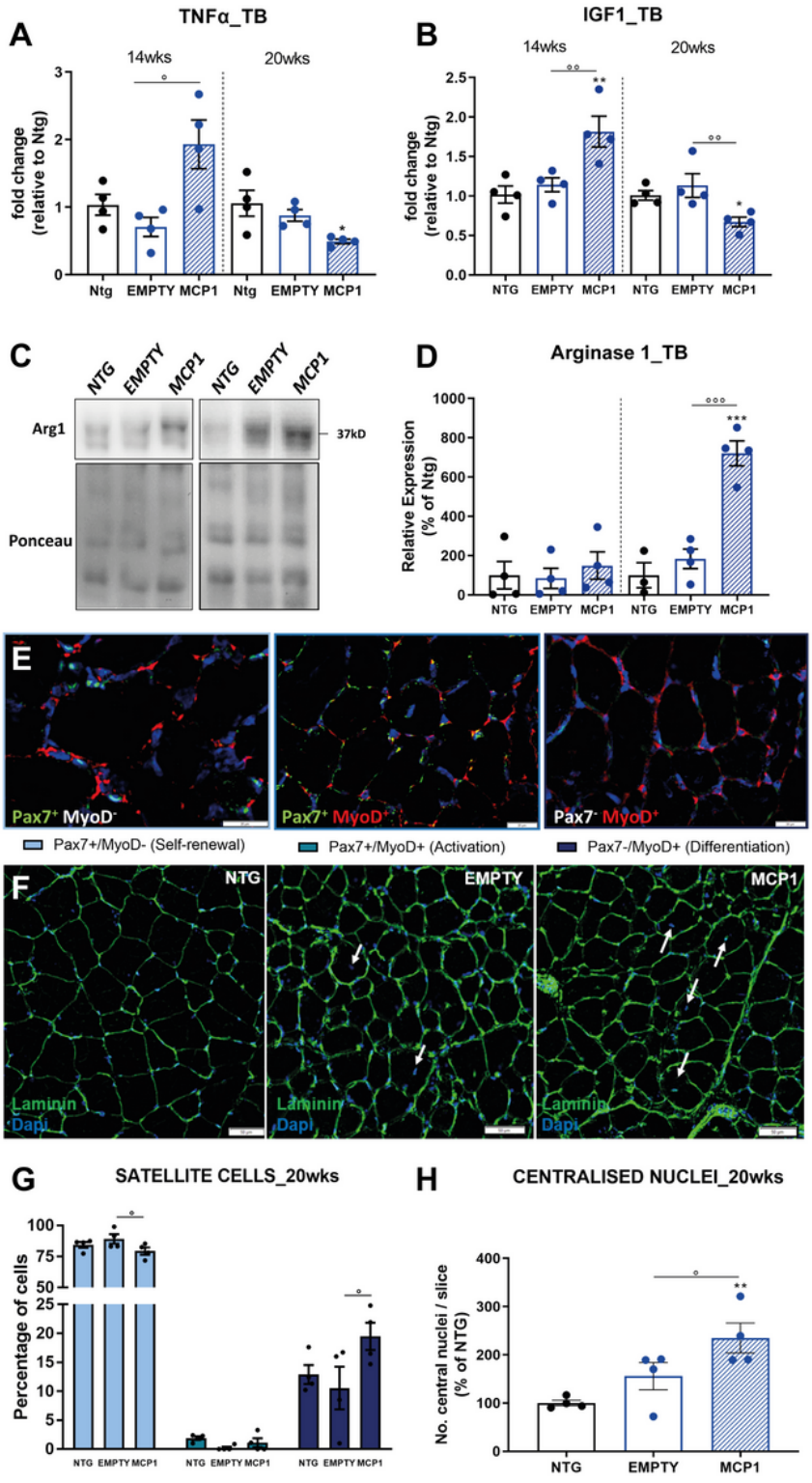

Figure 9

The MCP1-mediated immune response triggers the myogenic programme in the forelimb muscles of C57SOD1G93A mice. A, B Real-time PCR analysis of (A) Tnfα and (B) Igf1 transcript in the TB muscle of scAAV9_MCP1- and scAAV9(empty)-treated mice compared to relative Ntg littermates at 14 and 20 weeks. Data are normalised to β-actin and expressed as mean±SEM. n=4 per experimental group. C, D Representative immunoblot images and relative densitometric analysis of Arginase1 expression in TB

muscle extracts of scAAV9_MCP1- and scAAV9(empty)-treated mice and Ntg littermates at 14 and 20 weeks. Data are reported as mean±SEM. n=4 per group at each time point. E, F Confocal micrographs of coronal sections of TA muscle stained with (E) Pax7 (red), MyoD (green) and DAPI (blue) or (F) Laminin (green) and DAPI (blue) of symptomatic scAAV9_MCP1- and scAAV9(empty)-treated mice and Ntg littermates. Scale bar, (E) 20μm; (F) 50μm. G The analysis of satellite cells dynamic shows a decreased percentage of quiescent (Pax7+/MyoD-) and a compensatory increase of differentiating (Pax7-/MyoD+) myogenic progenitors in the TB muscle of scAAV9_MCP1-treated mice compared with the scAAV(empty) group at 20 weeks. H The morphometric analysis reveals an increased percentage of centralised myonuclei in the TB muscle of scAAV9_MCP1-treated mice compared with the scAAV9(empty) group at 20 weeks. Data are reported as mean±SEM of 3/5 serial sections per muscle from n=4 mice per experimental group. *p<0.05, **p<0.01, ***p<0.001 Ntg Vs MCP1; °p<0.05, °°p<0.01, °°°p<0.001 EMPTY Vs MCP1 by (A, B, D, H) one-way ANOVA or (G) two-way ANOVA with Fisher post-analysis.

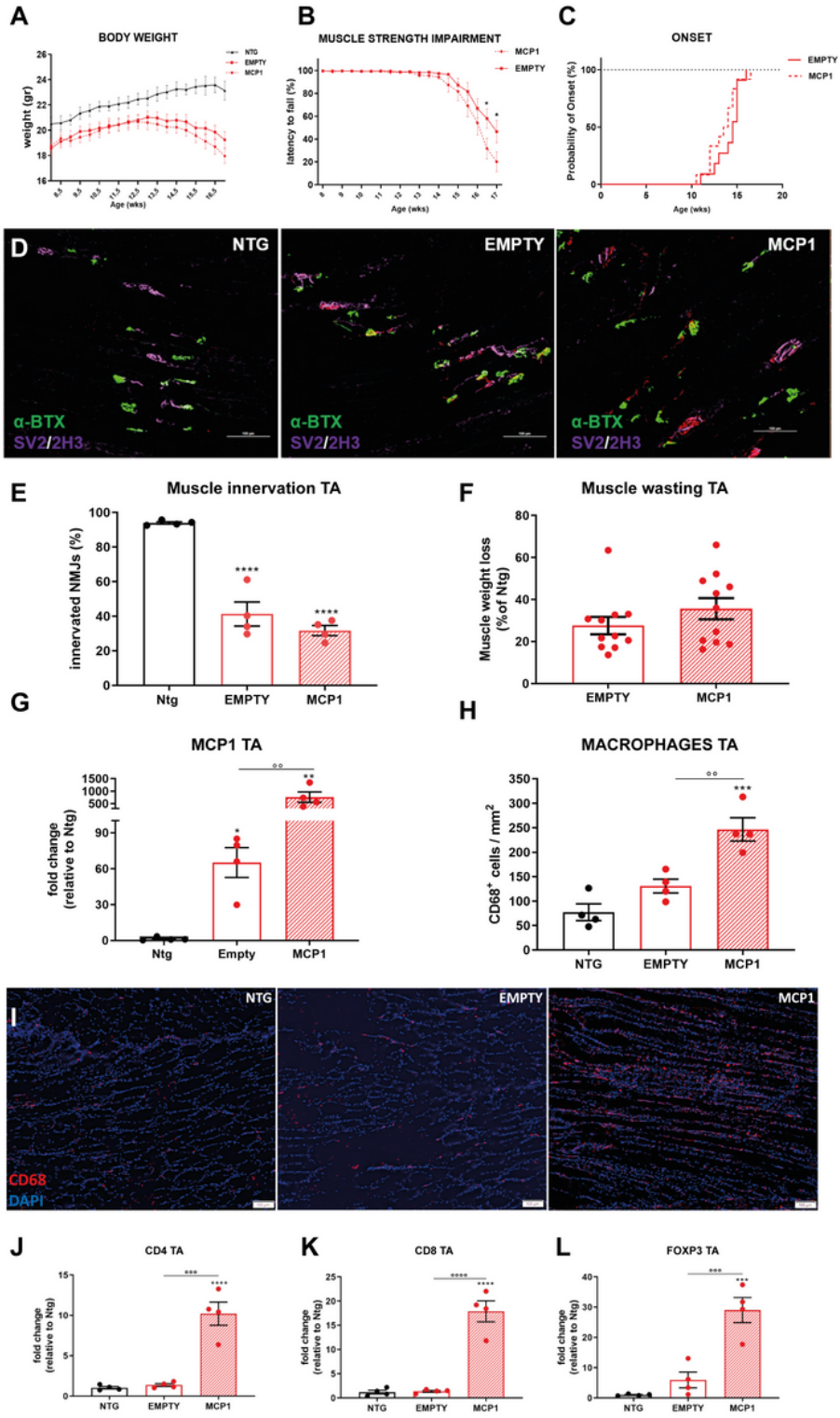

Figure 10

The scAAV9_MCP1 injection exacerbates the peripheral inflammatory response worsening the clinical phenotype of 129SvSOD1G93A mice. A-C Recording of (A) body weight and (B) muscle strength impairment of scAAV9_MCP1- and scAAV9(empty)-treated mice. Data are reported as mean±SEM for each time point. *p<0.05 by repeated-measures ANOVA with Sidak's post-analysis. (C) No difference in the disease onset was recorded between scAAV9_MCP1- and scAAV9(empty)-treated mice. p=0.8899 by

Mantel-Cox log-rank test. n=12 per group. D-F Representative micrographs of longitudinal TA muscle sections of scAAV9_MCP1- and scAAV9(empty)-treated mice and Ntg littermates at 17 weeks. α-Bungarotoxin (αBTX, green): postsynaptic terminal; synaptic vesicle glycoprotein2A (SV2, purple) + neurofilament (2H3, purple): presynaptic bouton; growth-associated protein43 (GAP43, red): regenerating axons. Scale bar, 100μm. No difference in (E) muscle innervation or (F) axon regeneration was recorded between the two groups of 129SvSOD1G93A mice. Data are reported as mean±SEM of 3/5 serial sections per muscle (~70 α-BTX+ endplates randomly taken) from n=4 per group. G No difference in muscle wasting was recorded between the two groups of 129SvSOD1G93A mice. Data are reported as mean±SEM. n=12 per group. H Real-time PCR analysis of Mcp1 transcript in the TA muscle of scAAV9_MCP1- and scAAV9(empty)-treated mice and Ntg littermates. Data are normalised to β-actin and expressed as mean±SEM. I, J Representative micrograph and relative quantification of TA muscle longitudinal sections of scAAV9_MCP1- and scAAV9(empty)-treated mice and Ntg littermates stained with the phagocytic marker CD68 (red) and DAPI (nucleus, blue). Scale bar, 100μm. Data are reported as mean±SEM of 3/5 serial sections per muscle from n=4 per group. K-M Real-time PCR analysis of (K) CD8a, (L) CD4 and (M) Foxp3 transcript in the TA muscle of scAAV9_MCP1- and scAAV9(empty)-treated mice than Ntg littermates at 17 weeks. Data are normalised to β-actin and expressed as mean±SEM. n=4 per experimental group. *p<0.05, **p<0.01, ***p<0.001, ****p<0.0001 Ntg Vs EMPTY or MCP1; °°p<0.01, °°°p<0.001, °°°°p<0.0001 EMPTY Vs MCP1 by one-way ANOVA with Fisher post-analysis.

Supplementary Files

This is a list of supplementary files associated with this preprint. Click to download.

- Fig.S1.tif
- Fig.S2.tif
- Fig.S3.tif
- Fig.S4.tif
- Fig.S5.tif
- Fig.S6.tif
- Fig.S7.tif
- Fig.S8.tif
- Fig.S9.tif